

# Whistler wave excitation and effects of self-focusing on ion beam propagation through a background plasma along a solenoidal magnetic field

Mikhail A. Dorf, Igor D. Kaganovich, Edward A. Startsev, and Ronald C. Davidson  
*Plasma Physics Laboratory, Princeton, New Jersey 08543, USA*

(Received 24 September 2009; accepted 3 December 2009; published online 3 February 2010)

This paper extends studies of ion beam transport through a background plasma along a solenoidal magnetic field by Kaganovich *et al.* [Phys. Plasmas **15**, 103108 (2008)] to the important regime of moderate magnetic field strength satisfying  $\omega_{ce} > 2\beta_b\omega_{pe}$ . Here,  $\omega_{ce}$  and  $\omega_{pe}$  are the electron cyclotron frequency and electron plasma frequency, respectively, and  $\beta_b = v_b/c$  is the directed ion beam velocity normalized to the speed of light. The electromagnetic field perturbations excited by the ion beam pulse in this regime are calculated analytically and verified by comparison with the numerical simulations. The degrees of beam charge neutralization and current neutralization are estimated, and the transverse component of the Lorentz force associated with the excited electromagnetic field is calculated. It is found that the plasma response to the ion beam pulse is significantly different depending on whether the value of the solenoidal magnetic field is below or above the threshold value specified by  $\omega_{ce}^{cr} = 2\beta_b\omega_{pe}$ , and corresponding to the resonant excitation of large-amplitude whistler waves. The use of intense whistler wave excitations for diagnostic purposes is also discussed. © 2010 American Institute of Physics. [doi:10.1063/1.3280013]

## I. INTRODUCTION

Neutralization and focusing of a charged particle beam by a background plasma form the basis for a variety of applications to high energy accelerators and colliders,<sup>1,2</sup> ion-beam-driven high energy density physics and fusion,<sup>3,4</sup> and astrophysics.<sup>5,6</sup> For instance, one of the modern approaches to ion beam compression for heavy ion fusion applications is to use a dense background plasma which charge neutralizes the ion charge bunch, and hence facilitates compression of the bunch against strong space-charge forces.<sup>3,4,7,8</sup> Additional control and focusing of the beam pulse can be provided by the application of a solenoidal magnetic field in the neutralizing region.<sup>9-13</sup> It has recently been demonstrated that even a weak magnetic field can significantly change the degrees of charge neutralization and current neutralization of an ion beam propagating through a background plasma.<sup>14,15</sup> In Refs. 14 and 15 detailed analysis of an ion beam propagating through a neutralizing plasma background along a solenoidal magnetic field has been performed for the regime of a weak applied magnetic field satisfying  $\omega_{ce} < 2\beta_b\omega_{pe}$ , where  $\omega_{ce}$  and  $\omega_{pe}$  are the electron cyclotron and plasma frequencies, respectively, and  $\beta_b = v_b/c$  is the directed ion beam velocity normalized to the speed of light  $c$ . In this paper, we extend earlier studies of nonrelativistic beam neutralization to the case where  $\omega_{ce} > 2\beta_b\omega_{pe}$ . An important difference between the two regimes appears to be due to excitation of electromagnetic wave-field perturbations, which propagate oblique to the beam axis for the case where the applied magnetic field exceeds the threshold value corresponding to  $\omega_{ce}^{cr} = 2\beta_b\omega_{pe}$ . Therefore, the slice approximation previously used for the analysis of the case where  $\omega_{ce} < 2\beta_b\omega_{pe}$  in Refs. 14 and 15, and not taking into account the effects of coupling between the longitudinal and transverse dynamics

cannot, in general, be applied in the present studies, and a different approach has to be developed. Note that the threshold value of the magnetic field can be expressed as  $B_c = 2\beta_b(n_p[\text{cm}^{-3}]/10^{11})^{1/2}$  kG. For instance, for an ion beam with  $\beta_b \sim 0.05$  propagating through a background plasma with density  $n_p \sim 10^{11} \text{ cm}^{-3}$ , this corresponds to a relatively weak magnetic field of 100 G.

In the present analysis, we consider a fast ion beam pulse with velocity much greater than the Alfvén velocity, and therefore the beam ions cannot interact effectively with ion Alfvén wave excitations. Furthermore, we assume a smooth beam density profile with a characteristic axial length scale for density variation,  $l_b$ , much greater than the wavelength of electron plasma wave excitations,  $l_b \gg v_b/\omega_{pe}$ . Therefore, electrostatic electron plasma wave excitations are also significantly suppressed.<sup>16,17</sup> However, if a sufficiently strong ambient magnetic field with  $\omega_{ce} > 2\beta_b\omega_{pe}$  is present inside the neutralizing region, the ion beam pulse can effectively interact with the electromagnetic electron whistler branch of the plasma dispersion relation.<sup>18,19</sup> Therefore, in the present paper we analyze excitation of the whistler branch by an ion beam pulse propagating through a neutralizing plasma along a solenoidal magnetic field and assess its influence on the degrees of beam charge neutralization and current neutralization, and the transverse beam dynamics.

The fundamental problem of whistler wave-field perturbations excited by a charged particle beam propagating in a magnetized plasma has been extensively studied for several decades, and various methods have been developed.<sup>19-24</sup> Recent interest in this problem has been motivated by possible use of charged particle beams for space communications. Propagating in the magnetized ionosphere or the magneto-

sphere plasma, charged particle beams can excite whistler wave-field perturbations, and therefore can be used as compact on-board emitters in the very-low-frequency range, replacing large-apertures electromagnetic antennas.<sup>19–21</sup> Analytical and numerical studies of whistler branch excitations by a density-modulated electron beam propagating through a background plasma along a uniform magnetic field, including both linear and nonlinear effects have been reported in Refs. 22–24. However, in those calculations the case of a thin beam with  $r_b \ll k_{\perp}^{-1}$  has been considered, and the effects of the transverse beam structure have not been taken into account. Here,  $r_b$  is the characteristic beam radius and  $k_{\perp}$  is the perpendicular component of the whistler wave vector. Note that in contrast with space-physics phenomena, where the wavelength of the whistler waves is large compared to the beam radius, for the parameters typical of neutralized intense ion beam transport applications, the beam radius can be comparable to the perpendicular wavelength. Furthermore, an axially continuous, density-modulated beam with modulation period  $l_m$  has been considered in Refs. 22–24, and therefore a monochromatic wave excitation with frequency  $\omega = v_b/l_m$  was obtained. Note that a finite-length ion beam pulse with a bell-shaped (not modulated) axial density profile used in intense beam transport applications can excite a broad frequency spectrum with a characteristic frequency  $\omega \sim v_b/l_b$  and bandwidth  $\delta\omega \sim \omega$ . Therefore, in the present analysis we consider excitation of the electromagnetic whistler branch by a finite-length ion beam pulse propagating through a background plasma along a solenoidal magnetic field, taking into account the effects of the longitudinal and transverse beam structures.

In the present paper we demonstrate that the total electromagnetic field excited by the ion beam pulse can be conveniently represented as the sum of two components: a *local* field component, corresponding to the local polarization of the background plasma, and rapidly decaying to zero outside the beam pulse, and a *wave* field component that can extend far outside the beam. It is then shown that in the regime where  $\omega_{ce} \gg 2\beta_b\omega_{pe}$  the local-field component has the dominant influence on the transverse beam dynamics. Moreover, in this limit, a positive charge of the ion beam pulse becomes overcompensated by the plasma electrons, resulting in an enhanced transverse focusing of the beam ions. Note that for the case where  $\omega_{ce} < 2\beta_b\omega_{pe}$  considered in Refs. 14 and 15, the beam charge is underneutralized, and the radial electric field has a defocusing effect. Furthermore, it is shown that the local plasma response is changing from paramagnetic for the  $\omega_{ce} < 2\beta_b\omega_{pe}$  case,<sup>14,15</sup> to diamagnetic for the  $\omega_{ce} > 2\beta_b\omega_{pe}$  case. The threshold value of the magnetic field  $\omega_{ce}^{cr} = 2\beta_b\omega_{pe}$ , which separates these qualitatively different regimes of ion beam interaction with the background plasma, corresponds to the resonant excitation of a large-amplitude wave-field component.<sup>22</sup>

It is important to point out that the effects of resonant wave excitation can be utilized for diagnostic purposes. Indeed, placing a pick-up loop outside the beam pulse and varying the amplitude of the applied magnetic field, a large-amplitude signal will be detected when the applied magnetic field approaches the threshold value specified by

$\omega_{ce}^{cr} = 2\beta_b\omega_{pe}$ . Therefore, it is expected that this scheme can be utilized as a passive diagnostic tool to measure the beam velocity or plasma density.

This paper is organized as follows. The theoretical model and assumptions in the present analysis are described in Sec. II. In Sec. III we consider the regime of resonant wave excitation, present the asymptotic time-dependent solution in the linear approximation, and estimate the saturation amplitude due to the nonlinear response of the plasma electrons. The analytical solutions for the electromagnetic field are compared with the results of numerical particle-in-cell (PIC) simulations in Sec. IV. Finally, in Sec. V a detailed analysis of the local field excitations, including the effects of enhanced beam self-focusing, is presented.

## II. THEORETICAL MODEL

In this section we calculate the electromagnetic field excitation generated by an ion beam pulse propagating through a cold background plasma with a constant velocity,  $v_b$ , along a uniform magnetic field  $\mathbf{B}_{\text{ext}} = B_{\text{ext}}\hat{z}$ . The beam carries a current  $j_b = Z_b e v_b n_b(z - v_b t, x)$ , where  $Z_b$  is the beam ion charge state,  $-e$  is the electron charge,  $n_b$  is the beam number density, and  $x$  and  $z$  are the transverse and longitudinal coordinates, respectively. For simplicity in the analytical studies, we consider here two-dimensional (2D) slab ( $x, z$ ) geometry, and the results of numerical simulations in cylindrical ( $r, z$ ) geometry are presented in Sec. IV. Provided the beam density is small compared to the plasma density ( $n_b \ll n_p$ ), we assume a linear (small-signal) plasma response and obtain the following equation for the Fourier transforms of the perturbed electromagnetic field components  $\mathbf{E} = \int d\mathbf{k} d\omega \mathbf{E}_{\omega, \mathbf{k}} \times \exp(-i\omega t + ik_x x + ik_z z)$  and  $\mathbf{B} = \int d\mathbf{k} d\omega \mathbf{B}_{\omega, \mathbf{k}} \exp(-i\omega t + ik_x x + ik_z z)$ :<sup>25</sup>

$$k^2 \mathbf{E}_{\omega, \mathbf{k}} - \mathbf{k}(\mathbf{k} \cdot \mathbf{E}_{\omega, \mathbf{k}}) - \frac{\omega^2}{c^2} \vec{\epsilon} \cdot \mathbf{E}_{\omega, \mathbf{k}} = \frac{4\pi i \omega}{c^2} \mathbf{j}_{\omega, \mathbf{k}}. \quad (1)$$

Here,  $\vec{\epsilon}$  is the dielectric tensor describing linear response of the cold plasma electrons<sup>25</sup> with  $\epsilon_{xx} = \epsilon_{yy} = 1 - \omega_{pe}^2/(\omega^2 - \omega_{ce}^2)$ ,  $\epsilon_{zz} = 1 - \omega_{pe}^2/\omega^2$ , and  $\epsilon_{xy} = -\epsilon_{yx} = i\omega_{pe}^2\omega_{ce}/[\omega(\omega^2 - \omega_{ce}^2)]$ , where  $\omega_{pe} = (4\pi e^2 n_p/m_e)^{1/2}$  is the plasma frequency,  $\omega_{ce} = eB_{\text{ext}}/m_e c$  is the electron cyclotron frequency, and the plasma ion response is neglected provided  $\omega \gg \sqrt{\omega_{ce}\omega_{ci}}$ .<sup>26</sup> Here,  $\omega_{ci} = eB_{\text{ext}}/m_i c$  is the ion cyclotron frequency, and  $m_e$  and  $m_i$  are the electron mass and ion mass, respectively. Finally, we neglected perturbations in the ion beam motion, assuming that the time duration of beam-plasma interaction is smaller than the characteristic time for the ion beam response. The space-time Fourier transform of the beam current is specified by  $\mathbf{j}_{\omega, \mathbf{k}} = Z_b e v_b n_b(k_x, k_z) \delta(\omega - k_z v_b)$ , where  $n_b = \int d\xi dx n_b(x, \xi) \exp(-ik_x x - ik_z \xi)$ .

It is straightforward to show for this model of the beam current that Eq. (1) yields a steady-state solution, in which all quantities depend on  $z$  and  $t$  solely through the combination  $\xi = z - v_b t$ . In what follows, we assume that the beam pulse is sufficiently long, with  $r_b \ll l_b$  and  $\omega \sim v_b/l_b \ll \omega_{pe}$ . Note that the latter condition implies that electrostatic electron plasma wave excitations are significantly suppressed.<sup>16,17</sup> Finally, in this section, for simplicity we assume

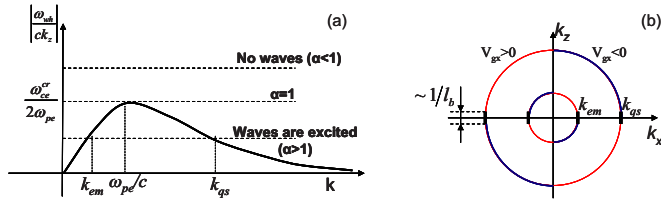


FIG. 1. (Color online) Plots of solutions to Eq. (7) corresponding to the wave vectors of the excited whistler wave field. (a) The absolute value of the normalized  $z$ -component of the whistler wave phase velocity (solid curve) is intersected by different values of the normalized beam velocity  $\beta_b$  (dashed lines). (b) The circles on the plane  $(k_x, k_z)$  illustrate the solutions to Eq. (7). For the case of a long beam pulse with  $l_b \gg k_{qs,w}^{-1}$ , the wave vectors primarily excited are illustrated by the short vertical bold lines. Red (thin) and blue (bold) colors illustrate positive and negative signs, respectively, of the  $x$ -component of the group velocity for the excited waves.

that  $\omega_{ce} \ll \omega_{pe}$ , and a general analysis for the case of an arbitrary ratio of  $\omega_{ce}/\omega_{pe}$  can be found in Appendix A. For present purposes, it is particularly important to analyze the  $x$ -component of the electric field perturbations,  $E_x$ , and the  $y$ -component of the magnetic field perturbations,  $B_y$ , which determine the transverse dynamics of the beam particles. After some straightforward algebra we obtain the following Fourier transforms of the transverse electromagnetic field components:

$$\frac{eE_{\omega,\mathbf{k}}^x}{m_e \omega_{pe} c} = -i \frac{c^3 Z_b k_x k^2 \omega_{ce}^2}{n_p \omega_{pe} (\omega_{pe}^2 + c^2 k^2)^2} \frac{k_z^2 v_b^2 n_{\mathbf{k}} \delta(\omega - k_z v_b)}{\omega^2 - \omega_{wh}^2(k_x, k_z)}, \quad (2)$$

$$\frac{eB_{\omega,\mathbf{k}}^y}{m_e \omega_{pe} c} = -i \frac{\beta_b Z_b \omega_{pe} c k_x}{n_p (\omega_{pe}^2 + c^2 k^2)} \frac{k_z^2 v_b^2 n_{\mathbf{k}} \delta(\omega - k_z v_b)}{\omega^2 - \omega_{wh}^2(k_x, k_z)}, \quad (3)$$

where use has been made of Faraday's equation,  $(\omega/c)\mathbf{B}_{\omega,\mathbf{k}} = \mathbf{k} \times \mathbf{E}$ , to obtain the perturbed magnetic field component. Here,  $\beta_b = v_b/c$ ,  $k^2 = k_x^2 + k_z^2$ , and

$$\omega_{wh}^2(k_x, k_z) = \frac{\omega_{ce}^2 k^2 k_z^2}{(k^2 + \omega_{pe}^2/c^2)^2}, \quad (4)$$

is the dispersion relation for the electron whistler branch. The electromagnetic field perturbations,  $E_x$  and  $B_y$ , can now be obtained by applying inverse space-time Fourier transforms to Eqs. (2) and (3). Integration over the frequency  $\omega$  readily gives

$$\frac{eE_{\mathbf{k}}^x}{m_e \omega_{pe} c} = -i \frac{c^3 Z_b k_x k^2 \omega_{ce}^2}{n_p \omega_{pe} (\omega_{pe}^2 + c^2 k^2)^2} \frac{k_z^2 v_b^2 n_{\mathbf{k}} \exp(-ik_z vt)}{k_z^2 v_b^2 - \omega_{wh}^2(k_x, k_z)}, \quad (5)$$

$$\frac{eB_{\mathbf{k}}^y}{m_e \omega_{pe} c} = -i \frac{\beta_b Z_b \omega_{pe} c k_x}{n_p (\omega_{pe}^2 + c^2 k^2)} \frac{k_z^2 v_b^2 n_{\mathbf{k}} \exp(-ik_z vt)}{k_z^2 v_b^2 - \omega_{wh}^2(k_x, k_z)}. \quad (6)$$

It is evident that the onset of wave-field generation by the beam pulse corresponds to existence of real solutions to

$$\omega_{wh}^2(k_x, k_z) = k_z^2 v_b^2. \quad (7)$$

Note that the condition in Eq. (7) is equivalent to the resonance condition for Cherenkov radiation, namely,  $V_z^{ph} = v_b$ , where  $V_z^{ph}$  is the  $z$ -component of the whistler wave phase velocity.

## A. Properties of the excited whistler waves

It is straightforward to show that real solutions to Eq. (7) exist, provided

$$\alpha = \omega_{ce}/2\beta_b \omega_{pe} > 1, \quad (8)$$

as illustrated in Fig. 1(a). For this case, the solutions  $k^2 = k_{em,qs}^2$  correspond to the long-wavelength electromagnetic part of the whistler branch,  $k = k_{em} < \omega_{pe}/c$ , and the short-wavelength quasioleostatic part,  $k = k_{qs} > \omega_{pe}/c$  [Fig. 1(a)]. In the limit where  $\alpha \gg 1$  the solutions are approximately given by

$$k_{qs} \cong \frac{2\alpha \omega_{pe}}{c}, \quad k_{em} \cong \frac{\omega_{pe}}{2\alpha c}. \quad (9)$$

Note that for a long beam pulse with  $k_z^{-1} \sim l_b \gg k_{qs,em}^{-1}$  the transverse wave vectors of the excited wave field are approximately given by  $k_x \approx \pm k_{qs,em}$  [see Fig. 1(b)].

The directions of the  $x$ -component of the group velocity  $V_{gx}$  for the excited wave field are illustrated in Fig. 1(b). Note that the quasioleostatic and the long-wavelength electromagnetic whistler waves with the same signs of phase velocity have opposite signs of group velocity,  $V_{gx}$ . Furthermore, it can be shown that the  $z$ -component of the group velocity for the short-wavelength quasioleostatic wave field is smaller than the beam velocity. In contrast, the long-wavelength electromagnetic wave field propagates in the  $z$ -direction faster than the beam. Therefore, the long-wavelength electromagnetic perturbations excited by the beam tail can propagate along the beam and influence the dynamics of the beam head. A schematic of the whistler wave excitations is shown in Fig. 2.

## B. Wave-field and local-field components of the excited electromagnetic perturbations

Wave-field excitations for the case where  $\alpha > 1$  are associated with the poles in Eqs. (5) and (6), which appear in the real space of the wave vector components  $(k_x, k_z)$ . Note, for the case of a long beam pulse,  $k_z^{-1} \sim l_b \gg k_{qs,em}^{-1}$ , that the pole locations on the real  $k_x$ -axis depend weakly on the value of  $k_z$ ,  $k_x \cong \pm k_{em,qs}(1 - k_z^2/2k_{em,qs}^2)$ . It is therefore convenient to carry out the inverse Fourier integration, first along the  $k_x$ -axis, and then along the  $k_z$ -axis. To properly account for the pole contributions, the integration over  $k_x$ -space should be carried out along the Landau contour,  $C_L$ , as illustrated in Fig. 3. Note that integration along the contour  $C_L$  shows that sufficiently far outside the beam only wave fields with a positive (negative)  $x$ -component of group velocity propagate in the region  $x > 0$  ( $x < 0$ ).

To demonstrate this fact, as an illustrative example, we consider the simple case where the spectrum of the beam density is an analytical function in the complex  $k_x$ -plane, which satisfies  $n_{\mathbf{k}} \exp(-|k_x x|) \rightarrow 0$  for large values of  $|k_x|$ . Considering  $x > 0$ , and closing the Landau contour through a semicircle of an infinitely large radius lying in the upper-plane [Figs. 3(a) and 3(b)], we readily obtain that the wave field excitations correspond to contributions from the poles at  $k_x = -k_{em}$  and  $k_x = k_{qs}$  for  $k_z < 0$ , and at  $k_x = k_{em}$  and  $k_x = -k_{qs}$  for  $k_z > 0$ . Note that the group velocity of these

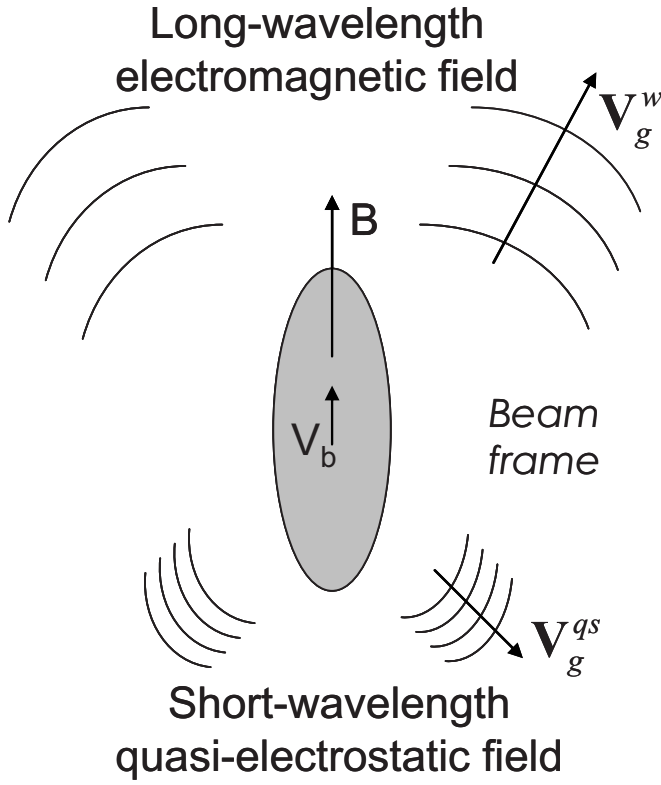


FIG. 2. Schematic of the whistler waves excited by the ion beam pulse. In the beam frame of reference, the long-wavelength electromagnetic wave-field propagates ahead of the beam pulse, and the short-wavelength quasiolestatic wave-field propagates toward the beam tail.

waves is indeed directed away from the beam, i.e.,  $V_{gx} > 0$  [see Fig. 1(b)]. Finally, it should be pointed out that the integration contours  $C_L$  are different for the cases where  $k_z > 0$  and  $k_z < 0$ . Therefore, even for a symmetric longitudinal beam density profile, the electromagnetic field perturbations are not, in general, symmetric around the beam center, implying oblique wave propagation.

For present purposes, it is convenient to represent the integration along the contour  $C_L$  for  $x > 0$  ( $x < 0$ ) as an integral along a slightly shifted upward (downward) contour  $C_+$  ( $C_-$ ) lying below (above) the poles of  $n_{\mathbf{k}}$ , plus (minus) the residues of the relevant on-axis poles [Figs. 3(c) and 3(d)]. For a beam with a smooth radial profile it can be shown that the contribution from the on-axis poles corresponds to the wave-field components of the electromagnetic field perturbation ( $E_x^W, B_y^W$ ) extending far outside the beam, and the integrals along the paths  $C_+$  and  $C_-$  correspond to the local-field components ( $E_x^{\text{loc}}, B_y^{\text{loc}}$ ) that rapidly decay to zero outside the beam. Assuming  $k_z \ll k_{em,qs}$  for a sufficiently long beam pulse, we obtain the following approximate expressions for the wave-field components of the electromagnetic field perturbation for  $x > 0$ ,

$$\frac{eB_y^W}{m_e \omega_{pe} c} = \frac{2\pi \omega_{pe} \beta_b Z_b}{c n_p (k_{qs}^2 - k_{em}^2)} (b_{em} + b_{qs}), \quad (10)$$

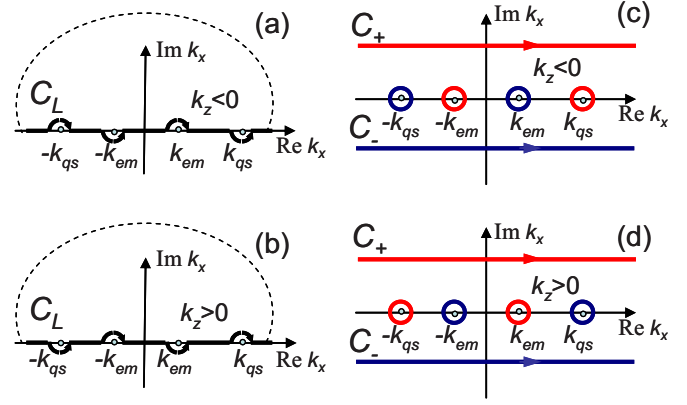


FIG. 3. (Color online) Integration contours used for evaluation of the integrals in Eqs. (5) and (6). Frames (a) and (b) show Landau contours  $C_L$  corresponding to  $k_z < 0$  and  $k_z > 0$ , respectively. Frames (c) and (d) illustrate contours of integration equivalent to the ones shown in frames (a) and (b), respectively. Red (gray) and blue (black) colors are used to illustrate the integration contours for  $x > 0$  and  $x < 0$ , respectively.

$$\frac{eE_x^W}{m_e \omega_{pe} c} = \frac{2\pi Z_b \omega_{ce}^2}{c n_p \omega_{pe} (k_{qs}^2 - k_{em}^2)} (e_{em} + e_{qs}). \quad (11)$$

Here,

$$b_{qs,em} = \pm (k_{qs,em}^2 + \omega_{pe}^2/c^2) \int_0^\infty dk_z n_{\mathbf{k}}(k_{qs,em}, k_z) \times \cos[k_z \xi \mp k_{qs,em} (1 - k_z^2/2k_{qs,em}^2)x], \quad (12)$$

$$e_{qs,em} = \pm k_{qs,em}^2 \int_0^\infty dk_z n_{\mathbf{k}}(k_{qs,em}, k_z) \times \cos[k_z \xi \mp k_{qs,em} (1 - k_z^2/2k_{qs,em}^2)x], \quad (13)$$

are the electric and magnetic components corresponding to the quasiolestatic (with subscript “qs”) and the long-wavelength electromagnetic (with subscript “em”) waves, respectively, and  $\xi = z - v_b t$ . Note that the correction term,  $\delta\varphi = (k_z^2/2k_{em,qs}^2)x$ , which we only retained in the phase of the wave-field component, yields a curvature in the phase fronts, and a corresponding decrease in the wave-field amplitude for  $x \approx l_b^2 k_{em,qs}$ . The local fields are given for  $x > 0$  by

$$\frac{eB_y^{\text{loc}}}{m_e \omega_{pe} c} = -i \int_{-\infty}^\infty dk_z e^{ik_z \xi} \int_{C_+} dk_x e^{ik_x x} n_{\mathbf{k}} \times \frac{\omega_{pe} \beta_b Z_b k_x (k_x^2 + \omega_{pe}^2/c^2)}{c n_p (k_x^2 - k_{em}^2)(k_x^2 - k_{qs}^2)}, \quad (14)$$

$$\frac{eE_x^{\text{loc}}}{m_e \omega_{pe} c} = -i \int_{-\infty}^\infty dk_z e^{ik_z \xi} \int_{C_+} dk_x e^{ik_x x} n_{\mathbf{k}} \times \frac{Z_b k_x^3 \omega_{ce}^2}{c n_p \omega_{pe} (k_x^2 - k_{em}^2)(k_x^2 - k_{qs}^2)}. \quad (15)$$

It should be noted that for the case where the beam density profile is specified by  $n_b(x, z - v_b t) = n_x(x) n_z(z - v_b t)$ , the integration over the  $k_z$ -space can be carried out independently from the  $k_x$ -space integration. Therefore, the axial de-

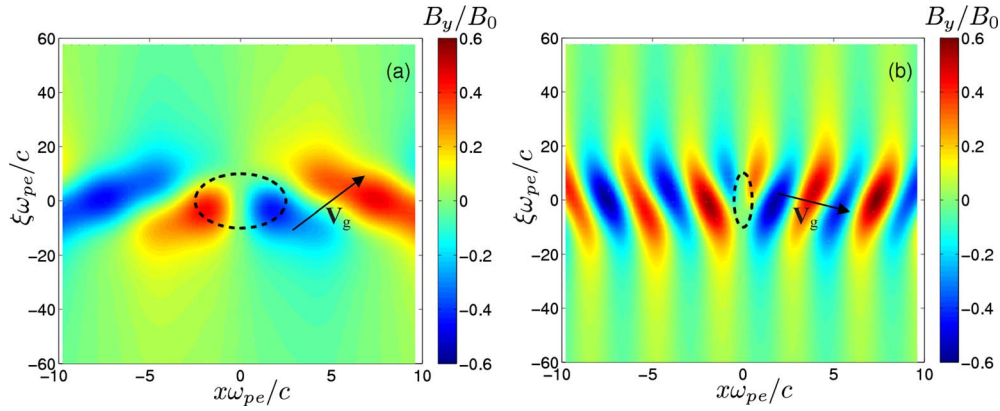


FIG. 4. (Color online) Plots of the steady-state amplitude of the transverse magnetic field perturbations  $B_y$ . The beam-plasma parameters correspond to  $Z_b = 1$ ,  $l_b = 10c/\omega_{pe}$ ,  $\beta_b = 0.33$ , and  $n_p = 2.4 \times 10^{11} \text{ cm}^{-3}$ . The applied magnetic field,  $B_{\text{ext}} = 1600 \text{ G}$ , corresponds to  $\alpha = \omega_{ce}/(2\beta_b\omega_{pe}) = 1.54$ . The frames show (a) primarily excitation of long-wavelength electromagnetic waves by a wide-aperture ion beam with  $r_b = 2.5c/\omega_{pe}$  and (b) primarily excitation of short-wavelength quasioleostatic waves by a thin beam with  $r_b = 0.5c/\omega_{pe}$ . The information used in obtaining the plots is obtained from Eqs. (A1)–(A7). The normalization factor in frames (a) and (b) is given by  $B_0 = 4\pi n_{b0} Z_b e \beta_b r_b$ . The arrows schematically illustrate the direction of the wave packet group velocity. Dashed lines correspond to the contour of constant beam density corresponding to the effective beam radius  $r_b$ .

pendence of the local fields is determined solely by the beam density axial profile, which is  $(E^{\text{loc}}, B^{\text{loc}}) = n_z(z - v_b t) \Phi_{E,B}(x)$ . In contrast, it is readily seen from Eqs. (10)–(13) that the wave field propagates obliquely to the beam. This implies a coupling between the transverse and longitudinal dynamics of the system, and therefore limits the validity of the slice approximation.

Features of the steady-state whistler wave excitation are shown in Fig. 4 for the following illustrative parameters:  $n_b = n_{b0} \exp[-r^2/r_b^2 - (z - v_b t)^2/l_b^2]$ ,  $l_b = 10c/\omega_{pe}$  (beam pulse duration  $\tau_b = l_b/v_b = 30.3/\omega_{pe}$ ),  $v_b = 0.33c$ ,  $n_{b0} = 0.05n_p$ ,  $n_p = 2.4 \times 10^{11} \text{ cm}^{-3}$ , and  $B_{\text{ext}} = 1600 \text{ G}$ . It is readily seen for a wide-aperture beam,  $r_b = 2.5c/\omega_{pe}$ , that the long-wavelength electromagnetic part of the whistler branch is primarily excited [Fig. 4(a)], and the amplitude of the quasioleostatic wave field is exponentially small [see Eq. (12)]. In contrast, for the case of a thinner beam,  $r_b = 0.5c/\omega_{pe}$ , the short-wavelength quasioleostatic waves are primarily represented in the excited spectrum [Fig. 4(b)] due to the large excitation factor,  $(k_{qs}^2 + \omega_{pe}^2/c^2)$ , in front of the integral in Eq. (12). Note that for the parameters in this illustrative example,  $\omega_{ce} \sim \omega_{pe}$ , and therefore to obtain the plots in Fig. 4, we used Eqs. (A1)–(A7), which include  $\omega_{ce}/\omega_{pe}$  correction terms.

### C. Time evolution of the wave-field perturbations

It should be noted that the denominators in Eqs. (10) and (11) can be expressed as

$$k_{qs}^2 - k_{em}^2 = 4\alpha\sqrt{\alpha^2 - 1}\omega_{pe}^2/c^2, \quad (16)$$

and it readily follows that there is strong resonant wave excitation for the case where the poles are merging, corresponding to  $\alpha = \omega_{ce}/2\beta\omega_{pe} = 1$  and  $k_{qs} = k_{em} = \omega_{pe}/c$  [see Fig. 1(a)]. Indeed, it can be shown in the limit  $\alpha = 1$  that the group velocity of an excited wave packet becomes equal to the beam velocity, i.e.,  $V_{gx} = 0$ ,  $V_{gz} = v_b$ . That is the wave packet

is moving together with the beam pulse, and can therefore be amplified to very large amplitude (during a very long time interval), assuming a linear plasma response. The wave-field intensity, however, will be saturated either by nonlinear processes or due to dissipation (collisions). Note that the local fields specified by Eqs. (14) and (15) do not have singularities at  $\alpha = 1$ .

For the case where  $\alpha > 1$ , the wave-field amplitude reaches a finite quasisteady-state limit with a characteristic time scale of  $\tau_s \sim \min\{r_b/V_{gx}, l_b/|V_{gz} - v_b|\}$ . This time interval is required for an initial transient wave packet to propagate sufficiently outside the beam pulse. For the excited wave vectors specified by Eq. (7), it can be shown that  $V_{gx}/(V_{gz} - v_b) = k_x/k_z$ . Therefore, for a sufficiently long beam pulse with  $l_b \gg k_{qs,em}^{-1}$ , the wave perturbations propagate primarily in the transverse direction and leave the beam in the time period  $\tau_s \sim r_b/V_{gx}$ . For the case where  $\alpha \geq 1$  and  $r_b \sim c/\omega_{pe}$ , making use of Eqs. (4) and (7), we obtain  $\tau_s \sim r_b/V_{gx} \sim l_b/v_b$ . That is, the time scale for achieving a quasisteady state is of order the beam pulse duration, and is therefore much longer than the plasma period, i.e.,

$$\tau_s \sim l_b/v_b \gg 1/\omega_{pe}. \quad (17)$$

Note that this result is significantly different from the case  $B_{\text{ext}} = 0$ , where the characteristic time to reach a quasisteady state is of order of the plasma period.

### D. Influence of the excited wave field on beam charge neutralization and current neutralization

It is of particular interest for neutralized beam transport applications to estimate the degrees of beam charge neutralization and current neutralization associated with the excited wave field. Here, we consider the case where  $\alpha \geq 1$ , and the limit where  $\alpha \gg 1$  and the analysis of the local-field component is addressed in Sec. V. It is convenient to introduce  $E_0 = 4\pi n_{b0} Z_b e r_b$  and  $B_0 = 4\pi n_{b0} Z_b e \beta_b r_b$  that represent, respectively, the characteristic transverse self-electric field and

self-magnetic field generated by an ion beam propagating in vacuum. Here,  $n_{b0}$  and  $r_b$  are the characteristic values of the beam density and radius. The degrees of beam charge neutralization and current neutralization can now be effectively measured by  $E_x/E_0$  and  $B_y/B_0$ . Considering, for simplicity, a Gaussian beam density profile with  $n_{\mathbf{k}}=(r_b l_b/4\pi)n_{b0} \exp[-r_b^2 k_x^2/4 - l_b^2 k_z^2/4]$ , it follows from Eqs.

(10)–(13) that the degrees of beam charge neutralization and current neutralization associated with the wave field excitations are given by

$$\frac{B_y^W}{B_0} \sim \sqrt{\pi} \frac{\max\{c^2 k_{qs}^2/\omega_{pe}^2 \exp(-r_b^2 k_{qs}^2/4), \exp(-r_b^2 k_{em}^2/4)\}}{4\alpha\sqrt{\alpha^2-1}}, \quad (18)$$

$$\frac{E_x^W}{E_0} \sim \sqrt{\pi} \frac{\omega_{ce}^2 \max\{(c^2 k_{qs}^2/\omega_{pe}^2) \exp(-r_b^2 k_{qs}^2/4), (c^2 k_{em}^2/\omega_{pe}^2) \exp(-r_b^2 k_{em}^2/4)\}}{\omega_{pe}^2 4\alpha\sqrt{\alpha^2-1}}. \quad (19)$$

It readily follows from Eqs. (18) and (19), for the case where  $r_b k_{em}/2 \leq 1$  and  $\alpha \geq 1$ , that the beam current is not neutralized, i.e.,  $B_y^W/B_0 \sim 1$ . The beam charge is, however, well neutralized, i.e.,  $E_x^W/E_0 \ll 1$ , provided  $\omega_{ce} \ll \omega_{pe}$  [this is due to the factor  $\omega_{ce}^2/\omega_{pe}^2$  in Eq. (19)]. For the case where  $\omega_{ce} \sim \omega_{pe}$ , the degree of charge neutralization decreases, giving  $E_x^W/E_0 \sim 1$  (see Appendix A), which is consistent with the analysis in Ref. 15.

### III. RESONANT WAVE EXCITATION: THE ASYMPTOTIC TIME-DEPENDENT SOLUTION

In the previous section, it was demonstrated for the critical case where  $\alpha=1$  that very-large-amplitude wave-field excitations are predicted by the linear theory for a quasisteady-state solution. This effect of large-amplitude wave-field excitations in the limit of merging poles corresponding to  $\alpha=\omega_{ce}/2\beta\omega_{pe}=1$  and  $k_{qs}=k_{em}=\omega_{pe}/c$  (so-called double pole case) has been previously reported in Refs. 22 and 23 for the case of an axially continuous and thin ( $r_b k_{\perp} \ll 1$ ) electron beam with a periodically modulated axial density profile. In those calculations, weak dissipation (due to collisions),<sup>22</sup> or nonlinear interaction between the beam electrons and the excited whistler waves,<sup>23</sup> was assumed in order to estimate the saturated amplitude of the electromagnetic field perturbations. In the present analysis we obtain the asymptotic time-dependent solution for the wave amplitude in the linear approximation. Furthermore, we discuss a possible mechanism for saturation of the wave field intensity associated with the nonlinear response of the background plasma electrons, which can drive the system off resonance. Provided the beam ions are sufficiently massive, the saturation determined by this mechanism can occur before the nonlinear interaction between the beam ions and the excited whistler waves becomes important.

To describe the time-evolution of the electromagnetic field perturbation excited by the ion beam pulse, we solve here an initial-value problem, making use of Laplace transforms with respect to time. Note that the temporal Fourier transform used in Sec. II yields only the steady-state solution. In this section, we assume that the initial electromagnetic field is zero everywhere, and the beam current

(source) is instantaneously turned on at  $t=0$ , i.e.,  $j_b=Z_b e n_b(z-v_b t, x)H(t)$ , where  $H(t)$  is the Heaviside step function defined by  $H(t)=0$  for  $t<0$ , and  $H(t)=1$  for  $t \geq 0$ . Similar to Eq. (3), we obtain that the space (Fourier)-time (Laplace) transform of the perturbed transverse magnetic field is given by

$$\frac{eB_{\omega, \mathbf{k}}^y}{m_e \omega_{pe} c} = -\frac{1}{2\pi} \frac{\omega_{pe} \beta_b^3 c^3 Z_b k_z^2 k_x n_{\mathbf{k}}}{n_p (\omega_{pe}^2 + c^2 k^2)} \times \frac{n_{\mathbf{k}}}{[\omega^2 - \omega_{wh}^2(k_x, k_z)](\omega - k_z v_b)}. \quad (20)$$

The inverse Laplace time transform performed in the complex  $\omega$ -plane readily gives

$$\frac{eB_{\mathbf{k}}^y}{m_e \omega_{pe} c} = -i \frac{\omega_{pe} \beta_b^3 c^3 Z_b k_z^2 k_x n_{\mathbf{k}}}{n_p (\omega_{pe}^2 + c^2 k^2)} \left[ \frac{\exp(-ik_z v_b t)}{k_z^2 v_b^2 - \omega_{wh}^2} + \frac{\exp(-i\omega_{wh} t)}{2\omega_{wh}(\omega_{wh} - k_z v_b)} + \frac{\exp(i\omega_{wh} t)}{2\omega_{wh}(\omega_{wh} + k_z v_b)} \right]. \quad (21)$$

Note that the first term inside the brackets in Eq. (21) corresponds to the steady-state solution [compare with Eq. (6)], in which all quantities depend on  $t$  and  $z$  exclusively through the combination  $\xi=z-v_b t$ . The other two terms describe the time evolution of the transient excitations. Assuming a sufficiently long beam pulse,  $k_z^{-1} \sim l_b \gg k_{qs, em}^{-1}$ , for the double-pole case corresponding to  $\alpha=\omega_{ce}/2\beta_b\omega_{pe}=1$ , Eq. (21) takes the form

$$\frac{eB_{\mathbf{k}}^y}{m_e \omega_{pe} c} = -i \frac{\omega_{pe} \beta_b^3 c^3 Z_b k_z^2 k_x n_{\mathbf{k}}}{2\omega_{wh} k_z v_b n_p} \times \left[ -\frac{\exp(-i\omega_{wh} t) - \exp(-ik_z v_b t)}{(k_x - \omega_{pe}/c)^2} + \frac{\exp(i\omega_{wh} t) - \exp(-ik_z v_b t)}{(k_x + \omega_{pe}/c)^2} \right]. \quad (22)$$

The right-hand side of Eq. (22) has two critical points on the real  $k_x$ -axis corresponding to  $k_x = \pm \omega_{pe}/c$ . However, for the case where  $\alpha=1$ , the dispersion relation yields  $\omega_{wh}(\pm \omega_{pe}/c, k_z) = \pm k_z v_b$ . Furthermore, the  $x$ -component of

the group velocity is equal to zero at the critical points,  $V_{gx}(k_x = \pm \omega_{pe}/c, k_z) = 0$ . Therefore, the time-dependent solution in Eq. (22) is regular at the critical points,  $k_x = \pm \omega_{pe}/c$ , and the inverse Fourier integration in  $k_x$ -space can be carried out along the real axis. Note that at large times,  $\omega_{wh}t \gg 1$ , the contribution to the integral comes mainly from the regions near the points of stationary phase, where  $\partial\omega_{wh}/\partial k_x \equiv V_{gx} = 0$ , which coincide with the critical points  $k_x = \pm \omega_{pe}/c$ . The asymptotic time-dependant solution is then given by

$$\begin{aligned} \frac{eB_{k_z}^y}{m_e\omega_{pe}c} &= -\frac{\omega_{pe}^2\beta_b Z_b e^{-ik_z v_b t}}{c^2 n_p} n_{\mathbf{k}}\left(\frac{\omega_{pe}}{c}, k_z\right) \\ &\times \sin\left(\frac{\omega_{pe}x}{c}\right) \int_{-\infty}^{\infty} d\Delta k_x \\ &\times \frac{\exp[i \operatorname{sgn}(k_z)\omega_{wh}''\Delta k_x^2 t/2] - 1}{\Delta k_x^2}, \end{aligned} \quad (23)$$

where  $B_{k_z}^y = \int_{-\infty}^{\infty} dk_x B_{\mathbf{k}}^y e^{ik_x x}$ ,  $\omega_{wh}'' = |[\partial^2\omega_{wh}/\partial k_x^2]_{k_x=\omega_{pe}/c}| = c^3|k_z| \times \beta_b/\omega_{pe}^2$ , and it has been assumed that  $n_{\mathbf{k}}(\omega_{pe}/c, k_z) = n_{\mathbf{k}}(-\omega_{pe}/c, k_z)$ . Noting that  $\int_{-\infty}^{\infty} dx [\exp(\pm ix^2) - 1]/x^2 = \sqrt{2\pi} \times (\pm i - 1)$ , we obtain

$$\frac{eB_y}{m_e\omega_{pe}c} = \sqrt{t} \frac{2\sqrt{\pi}\omega_{pe}v_b^{3/2}Z_b}{n_p} \sin\left(\frac{\omega_{pe}x}{c}\right) N_z(z), \quad (24)$$

where

$$N_z = \int_0^{\infty} dk_z \sqrt{k_z} n_{\mathbf{k}}\left(\frac{\omega_{pe}}{c}, k_z\right) [\cos(k_z \xi) + \sin(k_z \xi)], \quad (25)$$

and a symmetric beam profile with  $n_{\mathbf{k}}(\omega_{pe}/c, k_z) = n_{\mathbf{k}}(\omega_{pe}/c, -k_z)$  has also been assumed. Equations (24) and (25) describe the asymptotic evolution of the wave field for the double pole case corresponding to  $\alpha = \omega_{ce}/2\beta\omega_{pe} = 1$ . It is readily seen from Eq. (24) that at sufficiently large times,  $\omega_{wh}''t/r_b^2 \gg 1$ , the amplitude of the magnetic field is given by

$$B_y \sim \sqrt{v_b t/l_b Z_b} e n_b \beta_b r_b, \quad (26)$$

provided the beam radius is of the order of (or smaller than) the electron skin depth.

As the amplitude of the resonantly excited electromagnetic field perturbation increases, nonlinear processes can provide saturation of the energy transfer from the beam to the wave field. Here, we consider a plausible mechanism to describe saturation of the wave field intensity, in which the enhanced electromagnetic field perturbation generated by the ion beam pulse modifies properties of the whistler waves and drives the system off resonance. Indeed, as the longitudinal component of the magnetic field perturbation  $B_z$  increases, the resonance condition becomes less accurate,  $\alpha_{NL} = \omega_{ce}^{NL}/2\beta_b\omega_{pe} > 1$ , where  $\omega_{ce}^{NL} = e(B_0 + B_z)/m_e c$ . Recalling that the form of the resonant denominator is given by  $1/(\alpha\sqrt{\alpha^2-1})$ , the normalized magnitude of the perturbed longitudinal magnetic field  $\Delta\alpha \equiv (eB_z/m_e c)/(2\beta_b\omega_{pe})$  can be estimated by  $\Delta\alpha \sim Z_b(n_b/n_p)(r_b\omega_{pe}/c)[(1+\Delta\alpha^2)-1]^{-1/2}$  provided the beam radius is of the order of or smaller than the electron skin depth [see Eq. (B5)]. It now follows that the wave-field intensity saturates at the approximate level

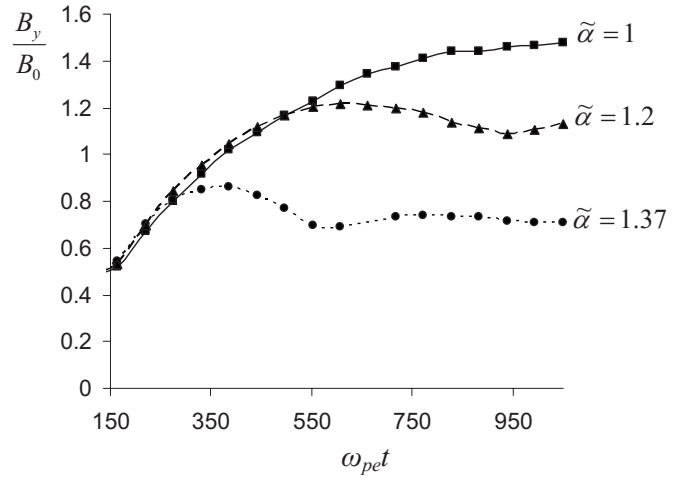


FIG. 5. Time evolution of the maximum value of the normalized perturbed transverse magnetic field plotted for different values of the applied magnetic field. The beam-plasma parameters correspond to  $Z_b=1$ ,  $r_b=0.92c/\omega_{pe}$ ,  $l_b=9.2c/\omega_{pe}$ ,  $\beta_b=0.33$ , and  $n_p=2.4 \times 10^{11} \text{ cm}^{-3}$ . The applied magnetic field corresponds to  $\tilde{\alpha}=1$  (solid curve),  $\tilde{\alpha}=1.2$  (dashed curve), and  $\tilde{\alpha}=1.37$  (dotted curve). The results are obtained using the 2D ( $x, z$ ) version of the LSP code.

$$\Delta\alpha \sim Z_b^{2/3}(n_b/n_p)^{2/3}(r_b\omega_{pe}/c)^{2/3}. \quad (27)$$

For the case of low beam density,  $n_b \ll n_p$ , this amplitude of the electromagnetic field perturbation is significantly higher compared to the case of nonresonant excitation,  $\alpha > 1$ , where the normalized steady-state amplitude is proportional to  $n_b/n_p$ . Finally, we emphasize that although the mechanism considered for the wave-field intensity saturation seems plausible, further detailed analytical and numerical studies are required to validate it.

The resonant excitation of whistler waves has been observed in numerical PIC simulations performed using the 2D slab ( $x, z$ ) version of the LSP code<sup>27</sup> taking into account electromagnetic effects. As an illustrative example, we consider a Gaussian ion beam pulse,  $n_b=0.05n_p \exp[-r^2/r_b^2 - (z-v_b t)^2/l_b^2]$ , with effective beam radius  $r_b=0.92c/\omega_{pe}$ , and beam pulse half length,  $l_b=9.2c/\omega_{pe}$  (beam pulse duration  $\tau_b=l_b/v_b=27.8/\omega_{pe}$ ), propagating with velocity  $v_b=0.33c$  through a background plasma with density,  $n_p=2.4 \times 10^{11} \text{ cm}^{-3}$ . In the numerical simulations, the ion beam is injected through the lower boundary of the simulation domain into an unperturbed magnetized plasma, and it propagates in the  $z$ -direction exciting electromagnetic field perturbations. Figure 5 shows the results of the numerical simulations for the time evolution of the maximum value of the perturbed transverse magnetic field  $B_y$ . Note that for the parameters in this illustrative example,  $\omega_{ce} \sim \omega_{pe}$  and  $\beta_b=0.33$ , and therefore a generalized analysis for arbitrary value of  $\omega_{ce}/\omega_{pe}$  should be carried out in order to estimate corrections to the resonance condition. The analysis shows (see Appendix A) that the resonant excitation of the wave field should occur at  $\tilde{\alpha} = \omega_{ce}(1-\beta_b^2)/(2\beta_b\omega_{pe}) = 1$ .<sup>14</sup> It is readily seen from Fig. 5 that as the magnitude of the applied uniform longitudinal magnetic field,  $B_{\text{ext}}$ , approaches the critical value corresponding to  $\tilde{\alpha}=1$ , the saturation amplitude of the perturbed magnetic field increases, as well as the time

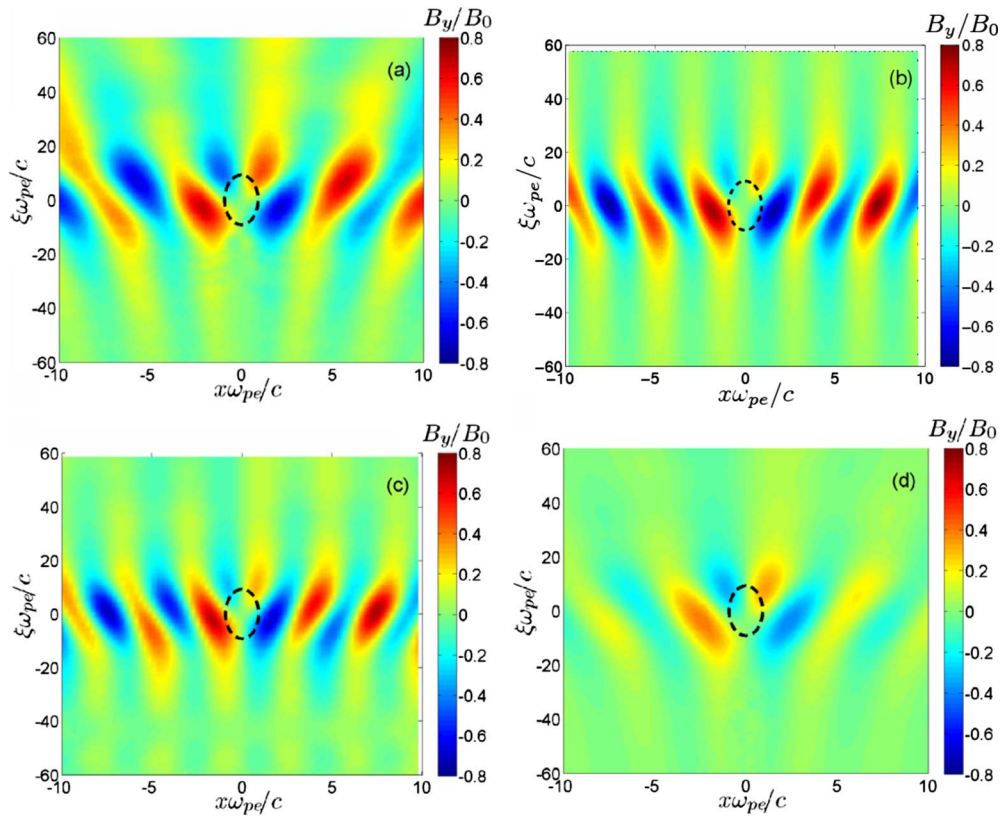


FIG. 6. (Color online) Plots of the steady-state amplitude of the transverse magnetic field perturbation  $B_y$ . The beam-plasma parameters correspond to  $Z_b = 1$ ,  $r_b = 0.92c/\omega_{pe}$ ,  $l_b = 10r_b$ ,  $\beta_b = 0.33$ , and  $n_p = 2.4 \times 10^{11} \text{ cm}^{-3}$ . The applied magnetic field,  $B_{\text{ext}} = 1600 \text{ G}$ , corresponds to  $\alpha = \omega_{ce}/(2\beta_b\omega_{pe}) = 1.54$ . The frames correspond to (a) results of numerical simulations obtained using the  $(x, z)$  slab version of the LSP code, (b) the analytical solution given by Eqs. (A1)–(A7), (c) numerical calculation of FFTs, assuming weak collisions  $\nu = 0.005/\tau_b$ , and (d) the results of numerical simulations obtained using the  $(r, z)$  cylindrical version of the LSP code. The dashed lines correspond to contours of constant beam density corresponding to the effective beam radius  $r_b$ .

interval required to achieve a quasisteady state. Note that the perturbed transverse magnetic field shown in Fig. 5 is normalized to the magnetic self-field of an unneutralized beam,  $B_0 = 4\pi n_{b0} Z_b e \beta_b r_b$ . It is evident, for the quasisteady-state regime, that the beam current is unneutralized,  $B_y \sim B_0$ , which is consistent with the analytical analysis performed in Sec. II.

Finally, it should be noted that the effect of resonant large-amplitude wave field excitations can be utilized for diagnostic purposes in experiments where an ion beam pulse propagates through a background plasma along an applied solenoidal magnetic field.<sup>3,7,8</sup> Indeed, measuring the perturbed azimuthal magnetic field, for instance, in the vicinity of the chamber wall, it can be expected to obtain the following dependence on the value of the applied magnetic field. First, at low values of the applied magnetic field,  $\alpha = \omega_{ce}/2\beta_b\omega_{pe} < 1$ , the wave-field component of the electromagnetic field perturbation is not excited, and the excited signal is exponentially small. As the magnetic field increases, and the threshold value of  $\alpha = \omega_{ce}/2\beta_b\omega_{pe} = 1$  is reached, a large-amplitude signal corresponding to resonant wave excitation will be detected. Finally, further increase in the magnitude of the applied magnetic field,  $\alpha = \omega_{ce}/2\beta_b\omega_{pe} > 1$ , will lead to a decrease in the amplitude of the excited signal. Provided the directed beam velocity is known, this diagnostic can be used, for instance, for passive measurements of the background plasma density. Indeed, determining the threshold magnitude of the applied magnetic field,  $B_c$ , from the

experimental data, the plasma density can be readily obtained from  $\omega_{pe} = \omega_{ce}(B_c)/2\beta_b$ .

#### IV. COMPARISON OF ANALYTICAL THEORY WITH NUMERICAL SIMULATIONS

In this section we present the results of the numerical simulations performed with the PIC code LSP and compare it with the analytical solutions described in Sec. II. Figure 6(a) shows the results obtained with the 2D slab  $(x, z)$  version of the code for the amplitude of the  $y$ -component of the perturbed magnetic field, when a quasisteady state is reached. The corresponding analytical solution [Eqs. (A1)–(A7)] is shown in Fig. 6(b). The following parameters have been used for this illustrative example:  $n_b = 0.05n_p \exp[-r^2/r_b^2 - (z - v_b t)^2/l_b^2]$ ,  $r_b = 0.92c/\omega_{pe}$ ,  $l_b = 10r_b$  (beam pulse duration  $\tau_b = l_b/v_b = 27.8/\omega_{pe}$ ),  $v_b = 0.33c$ ,  $n_p = 2.4 \times 10^{11} \text{ cm}^{-3}$ , and  $B_{\text{ext}} = 1600 \text{ G}$ . It is readily seen from Figs. 6(a) and 6(b) that the results of the numerical simulations and analytical theory are found to be in very good agreement. Indeed, the characteristic amplitude of the electromagnetic field perturbation, wavelength, angle of the propagation, etc., are quite similar.

In addition, to verify the approximate analytical solution specified by Eqs. (A1)–(A7), we first solved Eq. (1) for arbitrary values of  $\omega/\omega_{ce}$ ,  $\omega/\omega_{pe}$ , and  $\omega_{pe}/\omega_{ce}$ , and then numerically calculated the inverse *fast* Fourier transforms (FFTs). Note that in the regime where a wave field is excited,

the Fourier transforms of the perturbed electromagnetic fields contain singularities in real  $(k_x, k_z)$ -space. Therefore, the numerical integration of the FFT performed along the real  $k_x$ - and  $k_z$ -axes would diverge. To remove the singularities from the real axis, weak collisions have been assumed for the plasma electron response. Correspondingly, the components of the dielectric tensor,  $\vec{\epsilon}$ , should be modified according to<sup>25</sup>  $\epsilon_{xx} = \epsilon_{yy} = 1 - \omega_{pe}^2 (\omega + i\nu) / \{\omega[(\omega + i\nu)^2 - \omega_{ce}^2]\}$ ,  $\epsilon_{zz} = 1 - \omega_{pe}^2 / [\omega(\omega + i\nu)]$ , and  $\epsilon_{xy} = -\epsilon_{yx} = i\omega_{pe}^2 \omega_{ce} / \{\omega[(\omega + i\nu)^2 - \omega_{ce}^2]\}$ , where  $\nu$  is the effective collision frequency. In the limit of zero collision frequency, the numerical FFT calculation should yield the analytical solutions given in Eqs. (A1)–(A7). The results obtained in the numerical FFT calculation for the case of weak dissipation,  $\nu = 0.005 / \tau_b$ , demonstrate very good agreement with the analytical solution [compare Fig. 6(b) with Fig. 6(c)].

It is of particular interest to compare the results obtained for the case of  $(x, z)$  slab geometry [Figs. 6(a)–6(c)] to the case of cylindrical  $(r, z)$  geometry. The results of the numerical simulation obtained using the 2D  $(r, z)$  cylindrical version of the LSP code for the same system parameters are shown in Fig. 6(d). Results of the  $(r, z)$  LSP simulations demonstrate similar wavelength and propagation angle for the excited wave field. However, the amplitude of the perturbed electromagnetic field is smaller. Furthermore, it decays more rapidly outside the beam pulse, compared to the case of the slab beam pulse [compare Fig. 6(a) with Fig. 6(d)]. Note for an infinitely long beam that the amplitude of an excited electromagnetic field decreases as  $1/r$  for the case of cylindrical geometry, and does not decrease for the case of 2D slab geometry. This can provide a plausible explanation of the difference in the wave-field amplitude observed in cylindrical and slab geometries.

## V. SELF-FOCUSING OF AN INTENSE ION BEAM PULSE

In this section, making use of Eqs. (10)–(15), we calculate the transverse component of the Lorentz force,  $F_x = Z_b e E_x - Z_b e \beta_b B_y$ , acting on the beam particles. In Sec. II it has been shown that the excited wave field perturbations propagate oblique to the beam with characteristic longitudinal wave number  $k_z \sim l_b^{-1}$ . Therefore, the contribution of the wave-field component to the total Lorentz force can have opposite signs for the beam head and the beam tail. That is, it produces a focusing effect in the beam head and a defocusing effect in the beam tail, or *vice versa*. In contrast, the longitudinal profile of the local-field amplitude is the same as the longitudinal beam density profile (see Sec. II). Therefore, the local fields provide a focusing (or defocusing) effect over the entire length of the ion beam pulse. It is therefore important, in practical applications involving control over the beam aperture, to identify the parameter regimes where the local component of the electromagnetic field perturbation has the dominant influence on the beam transverse dynamics.

## A. Regimes of dominant influence of local fields on the beam transverse dynamics

It has been demonstrated in Sec. II for the critical case where  $\alpha = 1$  that a large-amplitude wave field is excited. Here, we consider the case where  $\alpha \gg 1$  ( $\omega_{ce} \gg 2\beta_b \omega_{pe}$ ). Furthermore, we assume  $r_b \gg k_{qs}^{-1}$ , or equivalently,  $r_b \gg c / (2\alpha \omega_{pe})$  in the limit where  $\alpha \gg 1$ . This implies an exponentially small level of the short-wavelength, quasioleostatic wave excitations for the case of a smooth radial beam density profile. Making use of Eqs. (10)–(13), it is straightforward to show for the case where  $r_b \gg k_{qs}^{-1}$  that the contribution of the wave-field component of the electromagnetic field perturbation to the transverse Lorentz force is given approximately by

$$F_x^W = Z_b e (E_x^W - \beta_b B_y^W) \approx 2\pi Z_b^2 \frac{m_e V_b^2}{R} \frac{1 - (4\alpha^2 - 1)k_{em}^2 c^2 / \omega_{pe}^2}{4\alpha \sqrt{\alpha^2 - 1}}, \quad (28)$$

where

$$\frac{1}{R} = \frac{\omega_{pe}^2}{c^2} \frac{1}{n_p} \int_0^\infty dk_z n_{\mathbf{k}}(k_{em}, k_z) \cos[k_z \xi + k_{em} x]. \quad (29)$$

Recall, for  $\alpha \gg 1$ , that the characteristic wave vector for the excited long-wavelength electromagnetic wave field is given by  $k_{em} = \omega_{pe} / 2\alpha c$ , and therefore the wave field contribution to the Lorentz force vanishes for  $\alpha \gg 1$ . To obtain the local field contribution, it is convenient to represent the local fields specified by Eqs. (14) and (15) in the following form:

$$e\beta_b B_y^{\text{loc}} = -iZ_b m_e v_b^2 \int d\mathbf{k} \frac{k_x (k_x^2 + \omega_{pe}^2 / c^2) n_{\mathbf{k}} e^{ik_x x + ik_z \xi}}{4\alpha \sqrt{\alpha^2 - 1} n_p} \times \left[ \frac{1}{k_x^2 - k_{qs}^2} - \frac{1}{k_x^2 - k_{em}^2} \right], \quad (30)$$

$$eE_x^{\text{loc}} = -iZ_b m_e v_b^2 \int d\mathbf{k} \frac{\alpha k_x^3 n_{\mathbf{k}} e^{ik_x x + ik_z \xi}}{\sqrt{\alpha^2 - 1} n_p} \times \left[ \frac{1}{k_x^2 - k_{qs}^2} - \frac{1}{k_x^2 - k_{em}^2} \right]. \quad (31)$$

For the case where

$$\alpha \gg 1 \quad \text{and} \quad r_b \gg k_{qs}^{-1} = \frac{c}{2\alpha \omega_{pe}}, \quad (32)$$

we can neglect by the first terms inside the brackets in Eqs. (30) and (31), and after some straightforward algebra we obtain that the local field contribution, which constitutes most of the transverse Lorentz force, is given by

$$F_x \approx Z_b e E_x^{\text{loc}} - Z_b e \beta_b B_y^{\text{loc}} = Z_b^2 m_e v_b^2 \frac{1}{n_p} \frac{dn_b}{dx}. \quad (33)$$

The analysis in Appendix A, performed for an arbitrary ratio of  $\omega_{ce} / \omega_{pe}$ , shows that for the case of a nonrelativistic ion beam the Lorentz force is still given by Eq. (33), provided

$$\alpha \gg 1 \quad \text{and} \quad r_b \gg \tilde{k}_{qs}^{-1} = (1 + \omega_{ce}^2/\omega_{pe}^2)^{1/2} \frac{c}{2\alpha\omega_{pe}}. \quad (34)$$

Note that the transverse component of the Lorentz force [Eq. (33)] is proportional to the gradient of the beam density. Therefore, for the case of a bell-shaped beam density profile, self-focusing of the beam occurs. Furthermore, it is interesting to note that an annular beam will not pinch to the axis provided the beam dynamics is governed by the force in Eq. (33). However, the outer beam radius will decrease and the inner beam radius will increase, resulting in a decrease in the thickness of the annulus and an increase in the beam density.

Although the total influence of the magnetic and electric field components,  $B_y^W$  and  $E_x^W$ , of the wave field perturbation results in a destructive interference in estimating the transverse Lorentz force [see Eq. (28)], it is of particular interest to estimate the separate contribution of the wave field component to the Lorentz force, and compare it with the contribution of the local field component. For illustrative purposes, we consider here a Gaussian beam density profile with  $n_{\mathbf{k}} = (r_b l_b / 4\pi) n_{b0} \exp[-r_b^2 k_x^2 / 4 - l_b^2 k_z^2 / 4]$ . Making use of Eqs. (10)–(13), it is straightforward to show that the contribution of the wave field component can be estimated by

$$eE_x^W \sim e\beta_b B_y^W \sim Z_b m_e v_b^2 \frac{\omega_{pe}^2 r_b n_{b0}}{\alpha^2 c^2 n_p} \exp\left(-\frac{r_b^2 k_{em}^2}{4}\right), \quad (35)$$

provided the conditions in Eq. (32) are satisfied. Similar expressions can be obtained for the local fields using Eqs. (30) and (31), i.e.,

$$eE_x^{\text{loc}} \sim Z_b m_e v_b^2 \frac{n_{b0}}{r_b n_p} \frac{1}{\max(1, k_{em}^2 r_b^2)}, \quad (36)$$

$$e\beta_b B_y^{\text{loc}} \sim Z_b m_e v_b^2 \frac{n_{b0}}{\alpha^2 r_b n_p} \frac{\max(1, \omega_{pe}^2 r_b^2 / c^2)}{\max(1, k_{em}^2 r_b^2)}. \quad (37)$$

It readily follows from Eqs. (35)–(37), for the case where the beam radius is small compared to the wavelength of the long-wavelength electromagnetic waves,  $r_b k_{em} \ll 1$ , that the *local electric field* has the dominant contribution to the transverse component of the Lorentz force. As the beam radius increases and becomes of order the electromagnetic wave-field wavelength,  $r_b k_{em} \sim 1$ , the separate contributions from all components of the perturbed electromagnetic field become of the same order, i.e.,  $E_x^{\text{loc}} \sim E_x^W \sim \beta_b B_x^{\text{loc}} \sim \beta_b B_x^W$ . With a further increase in the beam radius,  $r_b k_{em} \gg 1$ , the *local magnetic field* contribution becomes dominant, and both the quasioleostatic and long-wavelength electromagnetic wave-field components are excited to exponentially small levels for the case of a smooth beam density profile.

The time evolution of the electromagnetic field perturbation for the case where  $\alpha \gg 1$  and  $k_{qs}^{-1} \ll r_b \ll k_{em}^{-1}$ , which corresponds to a dominant influence of the local self-electric field, has been studied using the LSP simulation code. Figure 7 shows a plot of the perturbed transverse self-electric field at the simulation time  $t_s = 54$  ns. The beam-plasma parameters considered for this illustrative example correspond to  $n_b = 0.13 n_p \exp[-r^2/r_b^2 - (z - v_b t)^2/l_b^2]$ ,  $n_p = 10^{10} \text{ cm}^{-3}$ ,  $Z_b = 1$ ,  $r_b = 0.55c/\omega_{pe}$ ,  $\tau_b = 37.5/\omega_{pe}$ ,  $\beta_b = 0.05$ ,  $B_{\text{ext}} = 300$  G, and

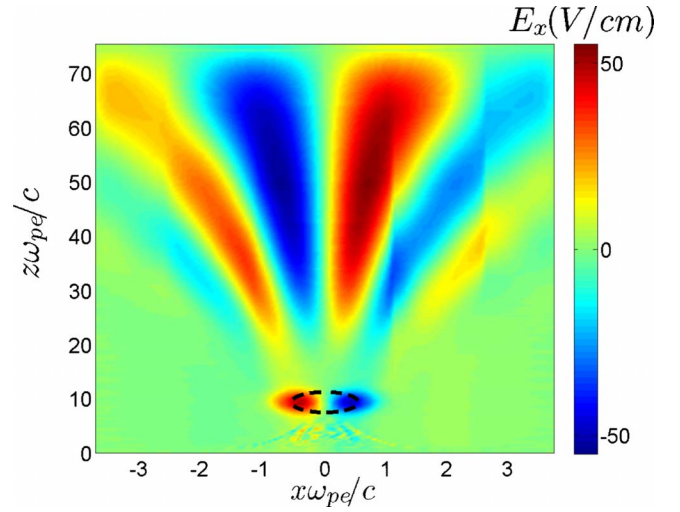


FIG. 7. (Color online) Plot of the perturbed transverse self-electric field corresponding to  $t_s = 54$  ns. The system parameters correspond to  $Z_b = 1$ ,  $r_b = 0.55c/\omega_{pe}$ ,  $\tau_b = 37.5/\omega_{pe}$ ,  $\beta_b = 0.05$ ,  $B_{\text{ext}} = 300$  G, and  $\alpha = \omega_{ce}/2\beta_b\omega_{pe} = 9.35$ . The results are obtained using the 2D  $(x, z)$  version of the LSP code. The dashed curve corresponds to the contour of constant beam density corresponding to the effective beam radius  $r_b$ .

$\alpha = \omega_{ce}/2\beta_b\omega_{pe} = 9.35$ . The wave structure in front of the beam pulse corresponds to a transient wave-field perturbations associated with the initial beam penetration into the plasma through the boundary at  $z = 0$ . Note that these transient perturbations do not interact with the ion beam pulse effectively, because they do not satisfy the Cherenkov criteria in Eq. (7). Therefore, the energy content in the corresponding wave field is attributed only to the initial beam penetration into the plasma, and is not related to the beam energy later in time. As the transient wave-field perturbations leave the beam on the characteristic time scale  $\tau_s \sim \min\{r_b/V_{gx}, l_b/|V_{gz} - v_b|\}$  (see Sec. II), the local component of the self-electric field exhibits the dominant influence on the ion beam transverse dynamics, as evident from Fig. 7. The intensity of the excited wave field satisfying the condition in Eq. (7) is negligible, which is consistent with the analytical calculations performed in this section.

## B. Enhanced ion beam self-focusing

In Sec. V A, it was demonstrated for the case where  $\alpha = \omega_{ce}/\beta_b\omega_{pe} \gg 1$  and  $r_b \gg c/(2\alpha\omega_{pe})$  that the local fields have the dominant influence on the transverse dynamics of the ion beam particles. In this regime, focusing is provided over the entire length of the beam pulse and the corresponding self-focusing force acting on the beam ions is specified by Eq. (33). It is of particular interest to compare this self-focusing force to the self-pinching force acting on the ion beam particles for the case where the ion beam pulse propagates through an unmagnetized plasma, i.e.,  $B_{\text{ext}} = 0$ . Indeed, even for this simple case, the beam charge is typically better neutralized than the beam current, and the self-pinching force is produced by the net self-magnetic field.<sup>28</sup> This self-pinching can be utilized for a variety of applications, including self-pinched ion beam transport<sup>29</sup> and heavy ion beam focusing.<sup>30</sup> Note that for the case where  $B_{\text{ext}} = 0$ , the beam

current is almost unneutralized in the limit where the beam radius is small compared to the electron skin depth,  $r_b \ll c/\omega_{pe}$ . Therefore, the self-pinching effect is a maximum in this regime.

For the case where  $r_b \ll c/\omega_{pe}$ , the ratio of the collective self-focusing force in the presence of an applied magnetic field [Eq. (33)] to the self-pinching force,  $F_0$ , in the limit  $B_{\text{ext}}=0$  case, can be estimated as  $F_x/F_0 \sim (c/r_b\omega_{pe})^2 \gg 1$ .<sup>31</sup> That is, the self-focusing of an ion beam pulse propagating through a neutralizing plasma can be significantly enhanced by the application of a solenoidal magnetic field satisfying  $\alpha = \omega_{ce}/2\beta_b\omega_{pe} \gg 1$ . Here, we emphasize again that the threshold value  $\alpha_{cr}=1$  typically corresponds to a weak magnetic field (see Introduction). The condition  $r_b \ll c/\omega_{pe}$  can be rewritten in terms of the beam current  $I_b$  as  $I_b \ll 4.25\beta_b(n_b/n_p)$  kA. Also, note that for a typical ion beam injector aperture of the order of 1 cm, the beam radius ( $\sim 1$  cm) is small compared to the electron skin depth provided the beam and plasma density are in the range of  $n_b < n_p < 2.8 \times 10^{11}/(r_b[\text{cm}])^2 \text{ cm}^{-3}$ , which are typical parameters for several beam transport applications.<sup>3,7,8</sup> Therefore, this self-focusing enhancement can be of considerable practical importance.

As a practical example, here we consider parameters characteristic of the present Neutralized Drift Compression Experiment (NDCX-I) (Ref. 7) and its future upgrade NDCX-II,<sup>8</sup> which are designed to study the energy deposition from the intense ion beam onto a target. The experiments involve neutralized compression of an intense ion beam pulse with radius  $r_b \sim 1$  cm as it propagates through a long drift section with length  $L_d \sim 200$  cm filled with a background plasma with density  $n_p \sim 10^{11} \text{ cm}^{-3}$ . As it exits the drift section, the beam passes through a strong magnetic lens with magnetic field  $B_s = 8$  T, and length  $L_s \sim 10$  cm, which provides additional transverse focusing. For the currently operating NDCX-I experiment, typical beam parameters correspond to  $\beta_b^I = 0.004$ ,  $m_i^I = 39$  a.u., and  $Z_b^I = 1$ . The proposed NDCX-II experiment is aimed at operating at higher beam energies:  $\beta_b^{II} = 0.032$ ,  $m_i^{II} = 7$  a.u., and  $Z_b^{II} = 1$ . The corresponding values of the critical magnetic field are given by  $B_c^I = 65$  G and  $B_c^{II} = 8$  G, for NDCX-I and NDCX-II parameters, respectively. The fringe magnetic field of the strong magnetic lens can penetrate deeply into the drift section at a magnitude much larger than  $B_c^{II}$ , thus providing conditions for enhanced self-focusing for both NDCX-I and NDCX-II. Moreover, the integrated effect of the beam self-focusing inside the drift section filled with the background plasma can become comparable to the focusing effect of the strong magnetic lens. Introducing the dimensionless parameters  $\delta = F_{sf}L_d/F_sL_s$ , where  $F_s \sim m_b\omega_{cb}^2 r_b/4$  is the magnetic focusing force acting on the beam ions inside the lens, and  $F_{sf} \sim m_e v_b^2/r_b$  is the self-focusing force ( $n_b \sim n_e$  is assumed), we readily obtain  $\delta^I = 0.04$  and  $\delta^{II} = 0.5$  for the parameters characteristic of NDCX-I and NDCX-II respectively. Here,  $m_b$  and  $\omega_{cb}$  are the ion beam mass and cyclotron frequency, respectively. Therefore, the plasma-induced collective focusing effect in a several hundred gauss magnetic field can be

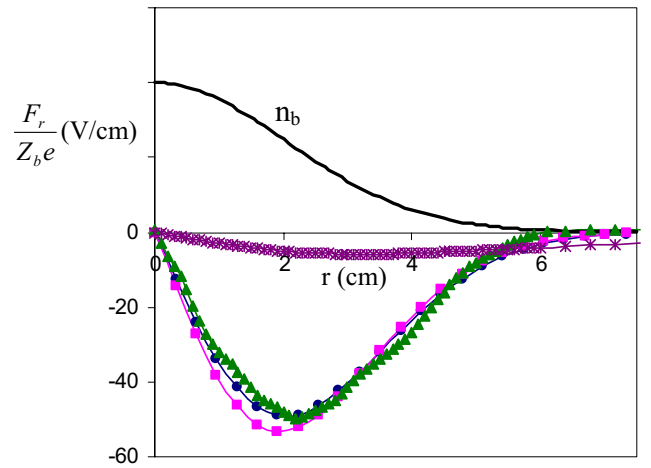


FIG. 8. (Color online) Radial dependence of the normalized focusing force at the beam center. The results of the numerical simulations correspond to  $B_{\text{ext}}=300$  G and  $\alpha = \omega_{ce}/2\beta_b\omega_{pe}=9.35$  (green triangles), and  $\omega_{ce}=0$  (purple stars). The analytical results in Eq. (32), are shown by the blue circles; the pink squares demonstrate the analytical predictions obtained by performing integration in Eqs. (A1)–(A7). The beam-plasma parameters correspond to  $Z_b=1$ ,  $r_b=0.55c/\omega_{pe}$ ,  $\tau_b=37.5/\omega_{pe}$ ,  $\beta_b=0.05$ , and  $n_p=10^{10} \text{ cm}^{-3}$ . The black curve corresponds to the radial beam density profile.

come comparable to the focusing effect of a strong 8 T final focus solenoid for the design parameters characteristic of NDCX-II.

It should be noted that Eq. (33), along with the conditions in Eq. (34), has been obtained previously in Ref. 31. The analysis in Ref. 31 was performed for the case of cylindrical geometry and assumed the slice approximation, which describes very well the local fields, and is of limited validity for the case where a strongly pronounced wave field perturbation is excited [see Sec. II]. Note that in this work we demonstrated the dominant influence of the local fields for the case where  $\alpha \gg 1$  and  $r_b k_{qs}^{-1} \gg 1$ , thus validating the assumptions used in the analysis in Ref. 31.

In addition, in the present work, the enhancement of the self-focusing force in the presence of a weak applied magnetic field has been observed in electromagnetic PIC simulations performed using the 2D ( $x, z$ ) slice version of the LSP code. As an illustrative example, we consider a Gaussian ion beam pulse,  $n_b = 0.13n_p \exp[-r^2/r_b^2 - (z - v_b t)^2/l_b^2]$ , with effective beam radius,  $r_b = 0.55c/\omega_{pe}$ , and beam pulse half-length,  $l_b = 1.875c/\omega_{pe}$  (beam pulse duration  $\tau_b = 37.5/\omega_{pe}$ ), propagating with velocity  $v_b = 0.05c$  through a background plasma with density  $n_p = 10^{10} \text{ cm}^{-3}$ . The results of the numerical simulations shown in Fig. 8 demonstrate the significant (approximately ten times) enhancement of the transverse component of the Lorentz force due to an applied magnetic field of  $B_{\text{ext}}=300$  G. Figure 8 shows the *total* transverse focusing force (i.e., the sum of the magnetic and electric component of the Lorentz force) acting on the beam ions in the presence of an applied magnetic field (green triangles, blue circles, and pink squares), and for the case where an external magnetic field is not applied (purple stars). The units of the electric field, V/cm, are chosen for practical representation of its numerical value. Note that the results of the numerical simulations are found to be in very good agreement with the

approximate analytical solution given by Eq. (33) (blue circles), and with the more accurate analytical solutions given by Eqs. (A1)–(A7) (pink squares).

### C. Properties of the local plasma response

As demonstrated above, the local component of the self-electric field provides the dominant contribution to the transverse Lorentz force for the case where  $\alpha = \omega_{ce}/2\beta_b\omega_{pe} \gg 1$  and  $k_{qs}^{-1} \ll r_b \ll k_{em}^{-1}$  (or equivalently,  $c/2\alpha\omega_{pe} \ll r_b \ll 2\alpha c/\omega_{pe}$ ). From Eq. (33) it now readily follows that

$$Z_b e E_x \approx Z_b^2 m_e v_b^2 \frac{1}{n_p} \frac{dn_b}{dx}, \quad (38)$$

and therefore, for the case of a bell-shaped beam density profile, the transverse electric self-field produces a focusing effect on the ion beam pulse. This implies that a positive charge of the ion beam pulse becomes *overcompensated* by the background plasma electrons.<sup>31</sup> In the same parameter regime, the  $z$ -component of the magnetic field perturbation is specified by (see Appendix B)

$$\frac{e B_z^{\text{loc}}}{m_e \omega_{pe} c} \approx - \frac{Z_b \beta_b^2 \omega_{pe}}{\omega_{ce} n_p} n_b(x, z), \quad (39)$$

indicating a diamagnetic plasma response.

It is interesting to note that a defocusing self-electric field and a paramagnetic plasma response was found for the case where  $\alpha < 1$ .<sup>14,15</sup> This means that the qualitatively different local plasma responses for the cases where  $\alpha < 1$  and  $\alpha > 1$  are separated by the critical case, corresponding to resonant excitation of a large-amplitude wave-field perturbation.

The analytical calculation demonstrating the dramatic change in the local plasma response with an increase in an applied magnetic field has also been verified by the results of 2D  $(x, z)$  LSP simulations (Fig. 9). The parameters chosen for the illustrative example in Fig. 9 correspond to  $n_b = 0.13 n_p \exp[-r^2/r_b^2 - (z - v_b t)^2/l_b^2]$ ,  $r_b = 0.55 c/\omega_{pe}$ ,  $l_b = 1.875 c/\omega_{pe}$ ,  $v_b = 0.05 c$ , and  $n_p = 10^{10} \text{ cm}^{-3}$ . One can readily see that the paramagnetic plasma response [Fig. 9(b)] and the defocusing effect of the transverse self-electric field [Fig. 9(a)] for the case where  $\alpha = 0.78$  change to a diamagnetic plasma response [Fig. 9(d)] and a focusing effect of the self-electric field [Fig. 9(c)] for  $\alpha = 9.35$ . Note that the longitudinal oscillations in Fig. 9(a) are an artifact of the numerical code, and a smooth longitudinal dependence can be obtained by increasing the space-time resolution along with the number of macroparticles. Figures 9(e) and 9(f) show the approximate analytical solutions for the transverse component of the electric field [Eq. (38)], and the longitudinal component of the magnetic field [Eq. (B4)], respectively. Finally, note that the magnitude of the transverse electric field perturbation is significantly increased by an increase in the applied magnetic field [compare Figs. 9(a) and 9(c)]. This strong transverse electric field provides the enhanced ion beam focusing, as discussed above.

## VI. CONCLUSIONS

In the present paper, the electromagnetic field perturbation excited by a long ion beam pulse propagating through a neutralizing background plasma along a solenoidal magnetic field was studied analytically and by means of numerical simulations using the electromagnetic PIC code LSP. It was demonstrated that the total electromagnetic field perturbation excited by an ion beam pulse with a smooth radial density profile can be conveniently represented as the sum of a local-field component, rapidly decaying to zero outside the beam pulse, and a wave-field component that can extend far outside the beam. The wave field is represented by a long-wavelength electromagnetic component with  $|k_x| = k_{em} < \omega_{pe}/c$ , and a short-wavelength quasioleostatic component with  $|k_x| = k_{qs} > \omega_{pe}/c$ . Note that the longitudinal component of the electromagnetic wave group velocity is greater than the beam velocity. Therefore, the long-wavelength electromagnetic perturbations excited by the tail of the beam pulse can propagate along the beam and influence the dynamics of the beam head. The system reaches a quasisteady state when the wave packet of the initial transient excitation propagates sufficiently far outside the beam. It was found, for a sufficiently long ion beam pulse, that the time scale for achieving a quasisteady state can be of order of the beam pulse duration, and is therefore much longer than the inverse plasma frequency. This result is significantly different from the case  $B_{\text{ext}} = 0$ , where the characteristic time to reach a steady state is of the order of the plasma period.

It was also shown that the wave-field excitations propagate obliquely to the beam with a characteristic wavelength of  $k_z \sim 1/l_b$ . Therefore, their contributions to the transverse component of the Lorentz force can have opposite signs for the beam head and the beam tail. In contrast, the longitudinal profile of the local-field amplitude is the same as the longitudinal beam density profile. Therefore, the transverse local fields have the same sign over the entire length of the ion beam pulse. It is therefore important, in practical applications involving control over the beam aperture, to identify the parameter regimes where the local component of the electromagnetic field perturbation has the dominant influence on the beam transverse dynamics.

In this paper, it was also demonstrated, in the regime where  $\omega_{ce} \gg 2\beta_b\omega_{pe}$  and  $r_b k_{qs} \gg 1$ , that the local-field component primarily determines the transverse dynamics of the beam particles, and the wave fields produce a negligible transverse force. Moreover, a positive charge of the ion beam pulse becomes overcompensated by the plasma electrons, and the associated strong transverse-focusing self-electric field has the dominant influence on the beam ions, compared to the magnetic field, provided  $k_{qs}^{-1} \ll r_b \ll k_{em}^{-1}$ . It was also shown, for the case where the beam radius is small compared to the electron skin depth, that the self-focusing force is significantly enhanced compared to the self-focusing force acting on the beam particles in the absence of an applied magnetic field. In addition, the local diamagnetic plasma response is observed in the numerical simulations and is also predicted analytically for  $\omega_{ce} \gg 2\beta_b\omega_{pe}$ . Note that these results differ significantly from the case  $\omega_{ce} < 2\beta_b\omega_{pe}$ , where

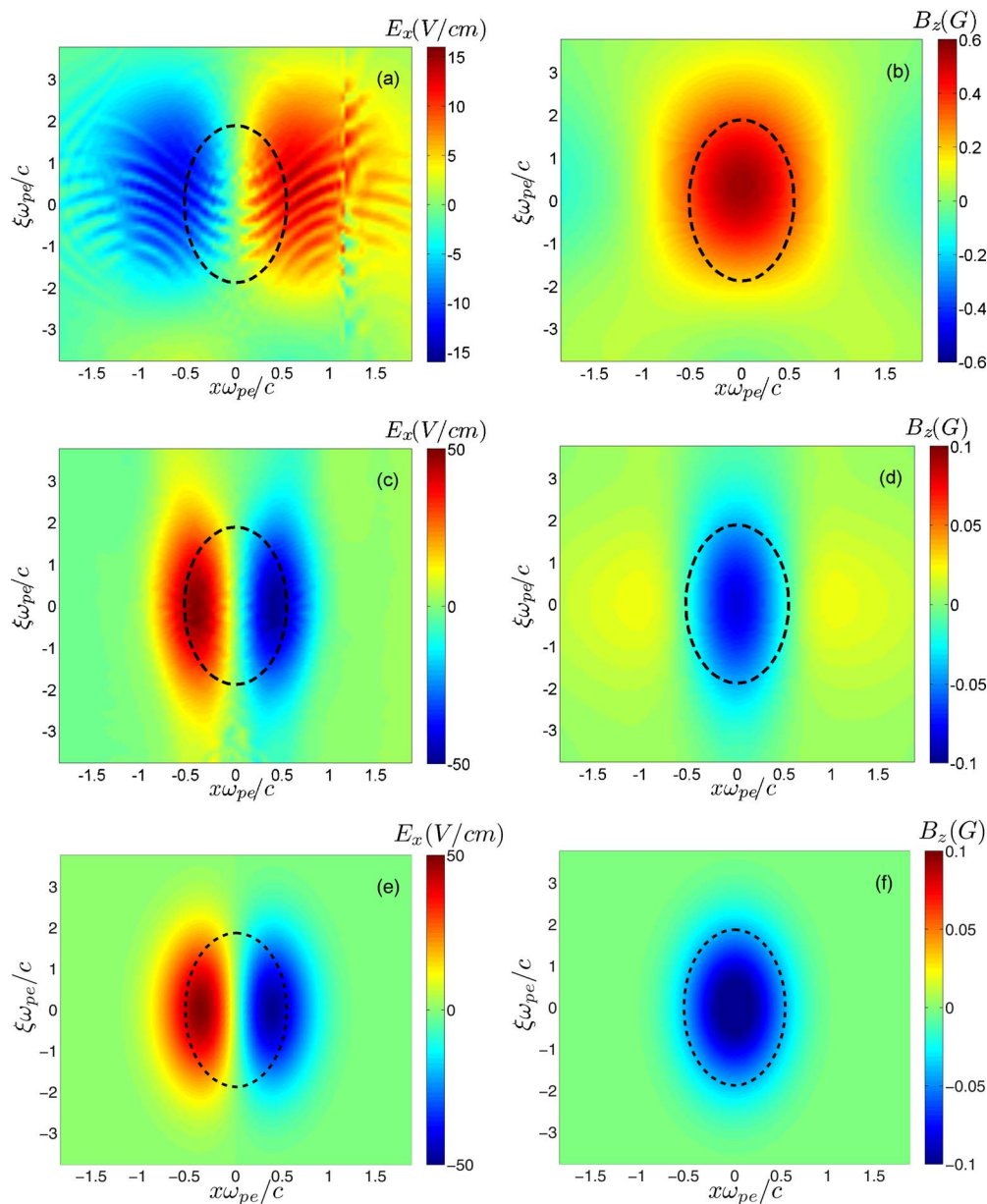


FIG. 9. (Color online) Plots of the transverse self-electric field (left) and longitudinal self-magnetic field (right) of an ion beam pulse with  $Z_b=1$ ,  $r_b=0.55c/\omega_{pe}$ ,  $l_b=1.875c/\omega_{pe}$ , and  $v_b=0.05c$  propagating through a background plasma with  $n_p=10^{10} \text{ cm}^{-3}$  along a solenoidal magnetic field. Frames (a) and (b) correspond to the results of 2D  $(x, z)$  LSP simulations for  $B_{\text{ext}}=25$  G. Frames (c) and (d) correspond to the results of 2D  $(x, z)$  LSP simulations for  $B_{\text{ext}}=300$  G. Frames (e) and (f) correspond to the approximate analytical solutions given by Eqs. (38) and (B4), respectively. Note the significantly different local plasma responses between the cases where  $\alpha=0.78$  [frames (a) and (b)] and  $\alpha=9.35$  [frames (c) and (d)]. Dashed lines correspond to contours of constant beam density corresponding to the effective beam radius  $r_b$ .

the transverse electric field is defocusing, and the plasma response is paramagnetic. The qualitatively different local plasma responses are separated by the critical field case where  $\omega_{ce}^{\text{cr}}=2\beta_b\omega_{pe}$ , corresponding to the resonant excitation of large-amplitude wave-field perturbations. In the present analysis, the asymptotic time-dependent solution was obtained for this critical case, and the saturation intensity of the wave-field perturbations, determined from the nonlinear response of the background plasma electrons, was estimated. In addition, a plausible application of the resonant wave excitation effect for diagnostic purposes was discussed.

Finally, we emphasize that the effects of an applied solenoidal magnetic field on neutralized ion beam transport

described in this paper for the case of  $\omega_{ce}>2\beta_b\omega_{pe}$  can be of particular importance for the presently operating NDCX-I (Ref. 7) and its future upgrade NDCX-II.<sup>8</sup> The design of the NDCX facilities first involves the neutralized drift compression of the ion beam pulse, and then additional transverse focusing on the target plane by a strong (several tesla) final-focus solenoid. The threshold magnetic field in the inequality  $\omega_{ce}>2\beta_b\omega_{pe}$  corresponds to a relatively weak magnetic field of the order of 10 G (for NDCX-I) and 100 G (for NDCX-II). Therefore, the magnetic fringe fields of the final-focus solenoid above this value can penetrate deep into the drift section. In particular, these fringe fields provide conditions for enhanced beam self-focusing, which can have a

significant influence on the transverse beam dynamics for the parameters characteristic of NDCX-II.

## ACKNOWLEDGMENTS

This research was supported by the U.S. Department of Energy under Contract No. DE-AC02-76CH-O3073 with the Princeton Plasma Physics Laboratory.

## APPENDIX A: ELECTROMAGNETIC FIELD PERTURBATIONS FOR THE CASE OF ARBITRARY RATIO OF $\omega_{ce}/\omega_{pe}$

Equations (10)–(15) can be generalized to the case of an arbitrary ratio of  $\omega_{ce}/\omega_{pe}$ . Assuming  $\omega \sim v_b/l_b \ll \omega_{pe}, \omega_{ce}$  and  $l_b \gg r_b, \tilde{k}_{em,qs}^{-1}$ , after some straightforward algebra one can show that the electromagnetic field perturbations for  $0 < x \ll l_b^2 \tilde{k}_{em,qs}$  are given by

$$\frac{eB_y^W}{m_e \omega_{pe} c} = \frac{2\pi \omega_{pe} \beta_b Z_b}{c n_p (\tilde{k}_{qs}^2 - \tilde{k}_{em}^2)} (b_{em} + b_{qs}), \quad (\text{A1})$$

$$\frac{eE_x^W}{m_e \omega_{pe} c} = \frac{2\pi Z_b \omega_{ce}^2}{c n_p \omega_{pe} (\tilde{k}_{qs}^2 - \tilde{k}_{em}^2)} (e_{em} + e_{qs}), \quad (\text{A2})$$

$$b_{qs,em} = \pm \left( \tilde{k}_{qs,em}^2 + \frac{\omega_{pe}^2}{c^2 (1 + \omega_{ce}^2/\omega_{pe}^2)} \right) \times \int_0^\infty dk_z n_{\mathbf{k}}(\tilde{k}_{qs,em}, k_z) \cos(k_z \xi \mp \tilde{k}_{qs,em} x), \quad (\text{A3})$$

$$e_{qs,em} = \pm [\tilde{k}_{qs,em}^2 (1 + \omega_{ce}^2/\omega_{pe}^2)] \times \int_0^\infty dk_z n_{\mathbf{k}}(\tilde{k}_{qs,em}, k_z) \cos(k_z \xi \mp \tilde{k}_{qs,em} x), \quad (\text{A4})$$

$$\frac{eB_y^{\text{loc}}}{m_e \omega_{pe} c} = -i \int_{-\infty}^\infty dk_z e^{ik_z \xi} \int_{C_+} dk_x e^{ik_x x} n_{\mathbf{k}} \times \frac{\omega_{pe} \beta_b Z_b k_x}{c n_p (k_x^2 - \tilde{k}_{em}^2)(k_x^2 - \tilde{k}_{qs}^2)} \left( k_x^2 + \frac{\omega_{pe}^2/c^2}{1 + \omega_{ce}^2/\omega_{pe}^2} \right), \quad (\text{A5})$$

$$\frac{eE_x^{\text{loc}}}{m_e \omega_{pe} c} = -i \int_{-\infty}^\infty dk_z e^{ik_z \xi} \int_{C_+} dk_x e^{ik_x x} n_{\mathbf{k}} \times \frac{Z_b k_x^3 \omega_{ce}^2 (1 + \omega_{ce}^2/\omega_{pe}^2)}{c n_p \omega_{pe} (k_x^2 - \tilde{k}_{em}^2)(k_x^2 - \tilde{k}_{qs}^2)}. \quad (\text{A6})$$

Here,  $\tilde{k}_{em,qs}$  are the solutions to the generalized dispersion relation

$$c^4 k_x^4 \left( 1 + \frac{\omega_{pe}^2}{\omega_{ce}^2} \right) + \left[ \frac{2\omega_{pe}^4}{\omega_{ce}^2} - \frac{(1 - \beta_b^2)\omega_{pe}^2}{\beta_b^2} \right] c^2 k_x^2 + \frac{\omega_{pe}^6}{\omega_{ce}^2} = 0. \quad (\text{A7})$$

Equations (A1)–(A7) describe the electromagnetic field perturbation excited by an ion beam pulse for an arbitrary ratio

of  $\omega_{ce}/\omega_{pe}$ , and furthermore for an arbitrary beam velocity, including the case of a relativistic ion beam. The dynamics of the background plasma electrons, however, are assumed to be nonrelativistic, which requires that the beam density be much smaller the plasma density ( $n_b \ll n_p$ ).

The onset of wave generation, corresponding to the existence of real solutions to Eq. (A7), is now determined by the condition  $\tilde{\alpha} = \omega_{ce}(1 - \beta_b^2)/2\beta_b \omega_{pe} > 1$ . In the limit where  $\tilde{\alpha} \gg 1$  and  $\beta_b \ll 1$ , the solutions to Eq. (A7) can be approximated by  $\tilde{k}_{qs} = 2\alpha \omega_{pe}/[c(1 + \omega_{ce}^2/\omega_{pe}^2)^{1/2}]$  and  $\tilde{k}_{em} = \omega_{pe}/(2\alpha c)$ , where  $\alpha = \omega_{ce}/2\beta_b \omega_{pe}$ . Making use of Eqs. (A1)–(A6), we can then reproduce the main results obtained earlier in the present paper. Repeating the analysis performed in Sec. III, after some straightforward algebra, we find that the asymptotic time-dependent solution for the critical case corresponding to  $\tilde{\alpha} = 1$  is given by

$$\frac{eB_y^v}{m_e \omega_{pe} c} = 4\sqrt{\pi} \sqrt{t} \frac{\beta_b^2 \tilde{k}_c \omega_{pe} Z_b \sin(\tilde{k}_c x) N_z(z)}{n_p (\tilde{k}_c^2 + \omega_{pe}^2/c^2) \sqrt{|\partial^2 \tilde{V}_{ph} / \partial k_x^2|_{k_x = \tilde{k}_c}}}, \quad (\text{A8})$$

$$N_z = \int_0^\infty dk_z \sqrt{k_z} n_{\mathbf{k}}(\tilde{k}_c, k_z) [\cos(k_z \xi) + \sin(k_z \xi)], \quad (\text{A9})$$

where the critical value of the wave vector,  $\tilde{k}_c$ , corresponding to the solution of Eq. (A7) for  $\tilde{\alpha} = 1$ , is given by

$$\tilde{k}_c = \left( \frac{1 + \beta_b^2 \omega_{pe}^2}{1 - \beta_b^2} \frac{1}{c^2 [1 + \omega_{ce}^2/\omega_{pe}^2]} \right)^{1/2}, \quad (\text{A10})$$

and the longitudinal component of the wave phase velocity is defined by

$$\tilde{V}_{ph}^z = \frac{\tilde{\omega}_{wh}}{k_z} = \frac{k_x \omega_c}{\sqrt{[k_x^2 + \omega_{pe}^2/c^2][k_x^2 (1 + \omega_{ce}^2/\omega_{pe}^2) + \omega_{pe}^2/c^2]}}. \quad (\text{A11})$$

Similarly, repeating the analysis performed in Sec. V, after some straightforward algebra one can demonstrate that for a nonrelativistic beam,  $\beta_b \ll 1$ , with  $r_b \tilde{k}_{qs} \gg 1$  and  $\alpha \gg 1$ , the total wave-field contribution to the transverse component of the Lorentz force vanishes, and the transverse force produced by the local field perturbation is still determined by Eq. (33), i.e.,

$$F_x = Z_b^2 m_e v_b^2 \frac{1}{n_p} \frac{dn_b}{dx}. \quad (\text{A12})$$

## APPENDIX B: AXIAL MAGNETIC FIELD PERTURBATION AND LOCAL DIAMAGNETIC PLASMA RESPONSE FOR $\alpha = \omega_{ce}/2\beta_b \omega_{pe} \gg 1$

Making use of Eq. (1) and the Faraday law, after some straightforward algebra, we find for an arbitrary ratio of  $\omega_{ce}/\omega_{pe}$  that the longitudinal component of the magnetic field perturbation is given by  $B_z = B_z^W + B_z^{\text{loc}}$ , where the local component,  $B_z^{\text{loc}}$ , and the wave component,  $B_z^W$ , are specified for  $0 < x \ll l_b^2 \tilde{k}_{em,qs}$  by

$$\frac{eB_z^W}{m_e\omega_{pe}c} = \frac{2\pi Z_b\omega_{ce}\omega_{pe}}{n_p(\tilde{k}_{qs}^2 - \tilde{k}_{em}^2)}(b_z^w + b_z^{qs}), \quad (\text{B1})$$

$$b_z^{em,qs} = [\tilde{k}_{em,qs}/(1 + \omega_c^2/\omega_p^2)] \int_0^\infty dk_z n_{\mathbf{k}}(\tilde{k}_{em,qs}, k_z) \times \sin(k_z z \pm \tilde{k}_{em,qs} x), \quad (\text{B2})$$

$$\frac{eB_z^{\text{loc}}}{m_e\omega_{pe}c} = \int_{-\infty}^\infty dk_z e^{ik_z z} \int_{C_+} dk_x e^{ik_x x} n_{\mathbf{k}} \times \frac{Z_b k_x^2 \omega_{ce} \omega_{pe} / (1 + \omega_c^2 / \omega_p^2)}{c^2 n_p (k_x^2 - \tilde{k}_{em}^2) (k_x^2 - \tilde{k}_{qs}^2)}. \quad (\text{B3})$$

It follows for the case of a nonrelativistic beam,  $\beta_b \ll 1$ , propagating through a background plasma with  $\alpha = \omega_{ce}/2\beta_b\omega_{pe} \gg 1$ , that the local  $z$ -component of the magnetic field perturbation is much greater than the wave-field  $z$ -component, and is given approximately by

$$\frac{eB_z^{\text{loc}}}{m_e\omega_{pe}c} \approx -\frac{Z_b\beta_b^2\omega_{pe}}{\omega_{ce}n_p} n_b(x, z), \quad (\text{B4})$$

provided the beam radius  $r_b$  satisfies  $\tilde{k}_{qs}^{-1} \ll r_b \ll \tilde{k}_{em}^{-1}$ , or equivalently,  $c(1 + \omega_c^2/\omega_p^2)/(2\alpha\omega_{pe}) \ll r_b \ll 2\alpha c/\omega_{pe}$  in the limit  $\alpha \gg 1$ . Equation (B4) demonstrates the diamagnetic plasma response, in accordance with the results obtained in the numerical simulations.

For the critical case where  $\alpha = \omega_{ce}/2\beta_b\omega_{pe} \approx 1$ , assuming a nonrelativistic ion beam,  $\beta_b \ll 1$ , after some straightforward algebra it follows from Eqs. (B1) and (B2) that  $\Delta\alpha \equiv (eB_z/m_e c)/(2\beta_b\omega_{pe})$  can be estimated by

$$\Delta\alpha \sim Z_b(n_b/n_p)(r_b\omega_{pe}/c)[(1 + \Delta\alpha^2) - 1]^{-1/2}, \quad (\text{B5})$$

provided the beam radius is of the order of or smaller than the electron skin depth. Note that in obtaining Eq. (B5), we used the fact that  $\omega_{ce} \ll \omega_{pe}$ , which is required by the resonance condition,  $\alpha = \omega_{ce}/2\beta_b\omega_{pe} = 1$ , for the case of a nonrelativistic ion beam pulse.

<sup>1</sup>P. Chen, J. M. Dawson, R. W. Huff, and T. Katsouleas, *Phys. Rev. Lett.* **54**, 693 (1985).

<sup>2</sup>C. Joshi, *Phys. Plasmas* **14**, 055501 (2007).

<sup>3</sup>P. K. Roy, S. S. Yu, E. Henestroza, A. Anders, F. M. Bieniosek, J. Coleman, S. Eylon, W. G. Greenway, M. Leitner, B. G. Logan, W. L. Waldron, D. R. Welch, C. Thoma, A. B. Sefkow, E. P. Gilson, P. C. Efthimion, and R. C. Davidson, *Phys. Rev. Lett.* **95**, 234801 (2005).

<sup>4</sup>S. S. Yu, R. P. Abbott, R. O. Bangerter, J. J. Barnard, R. J. Briggs, D. Callahan, C. M. Celata, R. Davidson, C. S. Debonnel, S. Eylon, A.

Faltens, A. Friedman, D. P. Grote, P. Heitzenroeder, E. Henestroza, I. Kaganovich, J. W. Kwan, J. F. Latkowski, E. P. Lee, B. G. Logan, P. F. Peterson, D. Rose, P. K. Roy, G.-L. Sabbi, P. A. Seidl, W. M. Sharp, and D. R. Welch, *Nucl. Instrum Methods Phys. Res. A* **544**, 294 (2005).

<sup>5</sup>M. V. Medvedev, M. Fiore, R. A. Fonseca, L. O. Silva, and W. B. Mori, *Astrophys. J. Lett.* **618**, L75 (2005).

<sup>6</sup>A. Gruzinov, *Astrophys. J. Lett.* **563**, L15 (2001).

<sup>7</sup>P. A. Seidl, A. Anders, F. M. Bieniosek, J. J. Barnard, J. Calanog, A. X. Chen, R. H. Cohen, J. E. Coleman, M. Dorf, E. P. Gilson, D. P. Grote, J. Y. Jung, M. Leitner, S. M. Lidia, B. G. Logan, P. Ni, P. K. Roy, K. Van den Bogert, W. L. Waldron, and D. R. Welch, *Nucl. Instrum Methods Phys. Res. A* **606**, 75 (2009).

<sup>8</sup>A. Friedman, J. J. Barnard, R. J. Briggs, R. C. Davidson, M. Dorf, D. P. Grote, E. Henestroza, E. P. Lee, M. A. Leitner, B. G. Logan, A. B. Sefkow, W. M. Sharp, W. L. Waldron, D. R. Welch, and S. S. Yu, *Nucl. Instrum Methods, Phys. Res. A* **606**, 6 (2009).

<sup>9</sup>R. Lee and R. N. Sudan, *Phys. Fluids* **14**, 1213 (1971).

<sup>10</sup>K. R. Chu and N. Rostoker, *Phys. Fluids* **16**, 1472 (1973).

<sup>11</sup>S. E. Rosinskii and V. G. Rukhlin, *Sov. Phys. JETP* **37**, 436 (1973).

<sup>12</sup>H. L. Berk and L. D. Pearlstein, *Phys. Fluids* **19**, 1831 (1976).

<sup>13</sup>J. C. Johnson, N. D'Angelo, and R. L. Merlini, *IEEE Trans. Plasma Sci.* **16**, 590 (1988).

<sup>14</sup>I. D. Kaganovich, E. A. Startsev, A. B. Sefkow, and R. C. Davidson, *Phys. Rev. Lett.* **99**, 235002 (2007).

<sup>15</sup>I. D. Kaganovich, E. A. Startsev, A. B. Sefkow, and R. C. Davidson, *Phys. Plasmas* **15**, 103108 (2008).

<sup>16</sup>I. D. Kaganovich, G. Shvets, E. Startsev, and R. C. Davidson, *Phys. Plasmas* **8**, 4180 (2001).

<sup>17</sup>I. D. Kaganovich, E. Startsev, and R. C. Davidson, *Phys. Plasmas* **11**, 3546 (2004).

<sup>18</sup>B. V. Oliver, D. D. Ryutov, and R. N. Sudan, *Phys. Plasmas* **1**, 3383 (1994).

<sup>19</sup>C. Krafft and M. Starodubtsev, *Planet. Space Sci.* **50**, 129 (2002) (and references therein).

<sup>20</sup>J. Lavernat and R. Pellat, *J. Geophys. Res.* **84**, 7223, doi:10.1029/JA084iA12p07223 (1979).

<sup>21</sup>C. Krafft, P. Thévenet, G. Matthieussent, B. Lundin, G. Belmont, B. Lembège, J. Solomon, J. Lavernat, and T. Lehner, *Phys. Rev. Lett.* **72**, 649 (1994).

<sup>22</sup>A. Volokitin, C. Krafft, and G. Matthieussent, *Phys. Plasmas* **2**, 4297 (1995).

<sup>23</sup>A. Volokitin, C. Krafft, and G. Matthieussent, *Phys. Plasmas* **4**, 4126 (1997).

<sup>24</sup>C. Krafft and A. Volokitin, *Phys. Plasmas* **5**, 4243 (1998).

<sup>25</sup>A. I. Ahiezer, I. A. Ahiezer, R. V. Polovin, A. G. Sitenko, and K. N. Stepanov, *Plasma Electrodynamics* (Nauka, Moscow, 1974).

<sup>26</sup>E. M. Lifshitz and L. P. Pitaevskii, *Physical Kinetics* (Pergamon, New York, 1981).

<sup>27</sup>LSP is a software product developed by ATK Mission Research, Albuquerque, NM 87110.

<sup>28</sup>I. D. Kaganovich, A. B. Sefkow, E. A. Startsev, R. C. Davidson, and D. R. Welch, *Nucl. Instrum Methods Phys. Res. A* **577**, 93 (2007).

<sup>29</sup>P. F. Ottinger, F. C. Young, S. J. Stephanakis, D. V. Rose, J. M. Neri, B. V. Weber, M. C. Myers, D. D. Hinshelwood, D. Mosher, C. L. Olson, and D. R. Welch, *Phys. Plasmas* **7**, 346 (2000).

<sup>30</sup>K. Hahn and E. Lee, *Fusion Eng. Des.* **32–33**, 417 (1996).

<sup>31</sup>M. Dorf, I. Kaganovich, E. Startsev, and R. Davidson, *Phys. Rev. Lett.* **103**, 075003 (2009).